



**UNIVERSIDAD DE INVESTIGACIÓN DE TECNOLOGÍA
EXPERIMENTAL YACHAY**

Escuela de Ciencias Físicas y Nanotecnología

**TÍTULO: ZIRCONIA DOPED CARBON NANOTUBES A
NANOSTRUCTURED SYSTEMS FOR BIOSENSOR APPLICATIONS**

Trabajo de integración curricular presentado como requisito para la obtención
del título de Ingeniero en Nanotecnología

Autor:

Jerez Masaquiza Marlon Danny

Tutor:

Ph.D. González Vásquez Gema

Urcuquí, agosto 2019



SUPPAN FLORES, GOTTFRIED ANDRES
Miembro No Tutor



CIFUENTES TAFUR, EVELYN CAROLINA
Secretario Ad-hoc

AUTORÍA

Yo, **MARLON DANNY JEREZ MASAQUIZA**, con cédula de identidad **1804625778**, declaro que las ideas, juicios, valoraciones, interpretaciones, consultas bibliográficas, definiciones y conceptualizaciones expuestas en el presente trabajo; así como, los procedimientos y herramientas utilizadas en la investigación, son de absoluta responsabilidad de el/la autora (a) del trabajo de integración curricular. Así mismo, me acojo a los reglamentos internos de la Universidad de Investigación de Tecnología Experimental Yachay.

Urcuquí, agosto 2019.



Marlon Danny Jerez Masaquiza

CI: 1804625778

AUTORIZACIÓN DE PUBLICACIÓN

Yo, **MARLON DANNY JEREZ MASAQUIZA**, con cédula de identidad **1804625778**, cedo a la Universidad de Tecnología Experimental Yachay, los derechos de publicación de la presente obra, sin que deba haber un reconocimiento económico por este concepto. Declaro además que el texto del presente trabajo de titulación no podrá ser cedido a ninguna empresa editorial para su publicación u otros fines, sin contar previamente con la autorización escrita de la Universidad.

Asimismo, autorizo a la Universidad que realice la digitalización y publicación de este trabajo de integración curricular en el repositorio virtual, de conformidad a lo dispuesto en el Art. 144 de la Ley Orgánica de Educación Superior

Urcuquí, agosto 2019.



Marlon Danny Jerez Masaquiza

CI: 1804625778

Acknowledgements

I am very grateful to my family for their support and encouragement over the five years of undergraduate studies.

I would like to express my appreciation to my advisor Dr. Gema González for providing me proper guidance on this project. Her passion in regard to research inspired me and made me succeed through a difficult time while I was working on this project. Without her guidance and persistent help, this thesis would not be possible.

I owe a particular thanks to Dr. Patricio Espinoza-Montero and Dr. Lenys Fernández for their help during the stay at laboratories of Pontificia Universidad Católica del Ecuador (PUCE).

In addition, a special acknowledge to Instituto de Fomento del Talento Humano (IFTH) for the scholarship during the undergraduate program.

Resumen

En este trabajo, se fabricó un biosensor de peróxido de hidrógeno basado en nanotubos de carbono (CNT), nanotubos dopados con zirconia (ZrO₂-CNTs), y azul de Prusia (PB). El electrodo de carbono vitreo (GC) fue modificado mediante ZrO₂-CNTs, y CNTs, luego PB fue electrodepositado. Se agregó el poli (cloruro de dialildimetilamonio) (PDDA) sobre cada capa para generar una estabilidad electrostática entre las capas de CNTs, ZrO₂-CNTs y PB. La morfología y estructura de los sistemas nanoestructurados fue caracterizado mediante microscopía electrónica de transmisión (TEM), difracción de rayos X (XRD) y espectroscopía infrarroja por transformada de Fourier (FTIR). Las propiedades electroquímicas fueron estudiadas mediante voltametría cíclica (CV) y amperometría. Los resultados experimentales indican que los electrodos modificados con CNT y ZrO₂-CNT exhiben procesos electroquímicos cuasi-reversibles, $i_{pa}/i_{pc} = 0.80$ y $i_{pa}/i_{pc} = 0.83$ a 40 mV/s. Sin embargo, el electrodo modificado con ZrO₂-CNTs podrían ser mejorando cambiando las condiciones de modificación y el método de síntesis. El sensor fabricado se puede utilizar para detectar eficientemente el peróxido de hidrógeno, presentando la buena relación lineal entre la concentración de peróxido de hidrógeno y la corriente máxima, una sensibilidad de 33.1 $\mu\text{A M}^{-1}$ y un límite de detección de aproximadamente 0.14 mM (S/N = 3).

Keywords: Biosensores; Nanotubos de carbono; Azul de Prusia; Nanopartículas de zirconia; Electroquímica.

Abstract

In this work, a hydrogen peroxide biosensor based on carbon nanotubes (CNTs), zirconia doped carbon nanotubes (ZrO₂-CNTs), and Prussian blue (PB) was fabricated. Glassy carbon (GC) electrode was modified by ZrO₂-CNTs, and CNTs, then PB was electrodeposited. Poly(diallyldimethylammonium chloride) (PDDA) was cast on each layer in order to have an electrostatic stability between the CNTs, ZrO₂-CNTs and PB layers. The morphology and structure of nanostructure system were characterized by transmission electron microscopy (TEM), X-ray diffraction (XRD) and Fourier transform infrared (FTIR) spectroscopy. The electrochemical properties were studied by cyclic voltammetry (CV) and amperometry. The experimental results indicate that both the CNTs and ZrO₂-CNTs modified electrodes exhibit quasi-reversible electrochemical processes, $i_{pa}/i_{pc} = 0.80$ and $i_{pa}/i_{pc} = 0.83$ at 40 mV/s. Nevertheless, ZrO₂-CNTs modified electrodes could be enhanced by changing the modification conditions and method of synthesis. The fabricated sensor can be used to efficiently detect hydrogen peroxide, presenting the good linear relationship between the hydrogen peroxide concentration and the peak current, a sensitivity of 33.1 $\mu\text{A M}^{-1}$ and a limit of detection of about 0.14 mM (S/N = 3).

Keywords: Biosensors; Carbon nanotubes; Prussian blue; Zirconia nanoparticles; Electrochemistry.

Contents

List of Figures	xvii
List of Tables	xx
I Introduction	1
I.I Problem Statement	2
I.II General Objectives	2
I.III Specific Objectives	3
1 Theoretical background	5
1.1 Biosensors	5
1.2 Hydrogen peroxide	6
1.3 Metal hexacyanoferrates: ferric hexacyanoferrate	6
1.4 Zirconium dioxide	7
1.5 Carbon nanotubes	8
1.5.1 Functionalization of carbon nanotubes	8
1.6 Nanostructured composite materials	10
1.6.1 Nanostructured materials composed of CNTs and metal oxides	10
1.6.2 Sol-gel method	11
1.7 Carbon nanotubes based electrochemical biosensors	11
1.8 Experimental techniques	12
1.8.1 Transmission electron microscopy (TEM)	12
1.8.2 Fourier transform infrared (FTIR) spectroscopy	12

1.8.3	X-ray diffraction (XRD)	13
1.8.4	Cyclic voltammetry (CV)	13
1.8.5	Chronoamperometry (CA)	16
2	Methodology	17
2.1	Reagents and solutions	17
2.1.1	Carbon nanotubes (CNTs) suspension	17
2.1.2	Poly(diallyldimethylammonium chloride) (PDDA) solution	18
2.1.3	Phosphate buffer saline (PBS) solution	18
2.2	Functionalization of carbon nanotubes	18
2.2.1	Prefunctionalization of carbon nanotubes (CNTs)	18
2.2.2	Functionalization of carbon nanotubes (CNTs)	18
2.2.3	Synthesis of ZrO ₂ -CNT nanostructured system	19
2.3	Physical and morphological characterization conditions	20
2.3.1	Transmission electron microscopy (TEM)	20
2.3.2	X-ray diffraction (XRD)	20
2.3.3	Fourier transform infrared (FTIR) spectroscopy	20
2.4	Electrochemistry	20
2.4.1	Analytic characterization	21
2.5	Preparation of modified electrodes	22
2.5.1	Preparation of carbon nanotubes (CNTs) modified electrodes	22
2.5.2	Preparation of Prussian blue (PB) based electrodes	22
2.6	Hydrogen peroxide (H ₂ O ₂) determination conditions	23
3	Results & Discussion	25
3.1	Structural and morphological characterization	25
3.1.1	Fourier transform infrared (FTIR) spectroscopy	25
3.1.2	X-ray diffraction (XRD) spectroscopy	27
3.1.3	Transmission electron microscopy (TEM)	29
3.1.4	Surface area BET	30
3.2	Electrochemical characterization of CNT based electrodes	30

3.2.1	Electron transfer behavior of glassy carbon (GC) electrode	30
3.2.2	Capacitance evaluation of glassy carbon (GC) electrode	32
3.2.3	Electron transfer behavior of PDDA/CNTs/GC electrode	33
3.2.4	Capacitance evaluation of PDDA/CNTs/GC electrode	35
3.2.5	Electron transfer behavior of PDDA/PB/PDDA/CNT/GC electrode	35
3.3	Electrochemical characterization of Zirconia-CNT based electrodes	38
3.3.1	Electron transfer behavior of PDDA/ZrO ₂ -CNTs/GC electrode	38
3.3.2	Capacitance evaluation of PDDA/ZrO ₂ -CNTs/GC electrode	39
3.3.3	Electron transfer behavior of PDDA/PB/PDDA/ZrO ₂ -CNTs/GC electrode	40
3.4	Electrochemical detection of hydrogen peroxide on the modified electrodes	43
3.4.1	Hydrogen peroxide detection in PDDA/CNTs/GC electrode	43
3.4.2	Hydrogen peroxide detection in PDDA/PB/PDDA/CNTs/GC electrode	44
3.4.3	Hydrogen peroxide detection in PDDA/ZrO ₂ -CNTs/GC electrode	46
3.4.4	Hydrogen peroxide detection in PDDA/PB/PDDA/ZrO ₂ -CNTs/GC electrode	47
4	Conclusions	51
	Bibliography	55
	Abbreviations	61

List of Figures

1.1	Cyclic voltammetry	14
1.2	Chronoamperometry diagrams	16
3.1	FTIR spectra of the CNT samples. Range: 4000 - 400 cm^{-1}	26
3.2	FTIR spectra of the CNT samples. Range: 1800 - 400 cm^{-1}	27
3.3	XRD pattern of the CNT samples	28
3.4	TEM images of the CNT samples	29
3.5	Electron transfer behavior of GC electrode	31
3.6	Capacitive behavior of GC electrode	33
3.7	Electron transfer behavior of PDDA/CNTs/GC electrode	34
3.8	Capacitive behavior of PDDA/CNTs/GC electrode	35
3.9	Electron transfer behavior of PDDA/PB/PDDA/CNTs/GC electrode	36
3.10	Cyclic voltammograms of modified electrodes	38
3.11	Electron transfer behavior of PDDA/ ZrO_2 -CNTs/GC electrode	39
3.12	Capacitive behavior of PDDA/ ZrO_2 -CNTs/GC electrode	40
3.13	Electron transfer behavior of PDDA/PB/PDDA/ ZrO_2 -CNTs/GC electrode	41
3.14	Cyclic voltammograms of ZrO_2 -CNTs based electrodes	43
3.15	PDDA/CNTs/GC electrode response to H_2O_2 presence	44
3.16	PDDA/PB/PDDA/CNTs/GC electrode response to H_2O_2	45
3.17	Amperometric studies of PDDA/PB/PDDA/CNTs/GC electrode	46
3.18	PDDA/ ZrO_2 -CNTs/GC electrode response to H_2O_2 presence	47
3.19	PDDA/PB/PDDA/ ZrO_2 -CNTs/GC electrode response to H_2O_2 presence	48

3.20 Amperometric studies of PDDA/PB/PDDA/ZrO ₂ -CNTs/GC electrode	49
---	----

List of Tables

2.1	Electrodeposition of PB	22
2.2	Stability evaluation of PB	23
3.1	XRD indexes of the CNT samples	28
3.2	XRD indexes of the ZrO ₂ samples	29
3.3	Diameter distribution of the CNT samples from TEM images	30
3.4	Characterization data of GC electrode	32
3.5	Characterization data of PDDA/CNTs/GC electrode	34
3.6	Characterization data of PDDA/PB/PDDA/CNTs/GC electrode	37
3.7	Characterization data of PDDA/ZrO ₂ -CNTs/GC electrode	39
3.8	Characterization data of PDDA/PB/PDDA/ZrO ₂ -CNTs/GC electrode	42

Chapter I

Introduction

Macrostructure systems-based biosensors have been widely studied in order to explore their potential applications in clinical diagnostics. The demand for biosensors for the detection of harmful biological agents has increased, and recent research is focused on ways of producing small portable devices that would allow fast, accurate, and on-site detection. Furthermore, the data given by biosensors is needed to be accurate and reliable, thus, electrochemistry and analytic chemistry combined with nanotechnology are promising areas of investigation in order to give the instrumentation, precise methodology and accurate diagnostic.[1]

Electrochemistry provides electroanalytical techniques which are widely used due to their rapid response, low cost, portability and facility to incorporate into complex systems. Electrochemical sensors are based on these techniques taking advantage of the redox processes of substances. A sensor is a device that transforms physicochemical changes and chemical processes (reduction/oxidation) into an analytical signal. It is made of a recognition element and a transducer. Recognition element interacts with the analyte and the transducer convert physicochemical changes into an electrical signal. In the case of biosensors, the recognition system is a biological element such as enzyme, antibody, microorganism, etc.[2]

Enzymes are substances which catalyze a chemical reaction. They only catalyze certain reactions because of their active site is selective, for instance glucose oxidase will catalyze only the reaction of glucose. Oxidase enzymes are often used as the recognition element. Unfortunately, enzyme based biosensors face the denaturation of the enzyme. Inorganic compounds which mimic the electrocatalytic activity of enzymes have been studied in recent years. Prussian blue (PB) as the transition metal hexacyanoferrates is one important group of inorganic compounds used in electrode modification and electrocatalytic purposes.[3] Moreover, PB is know as an artificial peroxidase,

and it is a promising candidate for the catalysis of hydrogen peroxide. The use of PB as a recognition element for hydrogen peroxide detection is extensive, for instance several studies have been reported. [4], [5], [6]

Furthermore, in order to increase the sensitivity and the rapid response of electrochemical sensors nanomaterials and nanostructure systems are used to modify the electrode surface. Since the discovery of carbon nanotubes (CNTs), researches have worked on their application in many fields. Nanotubes possess interesting chemical and physical properties which are useful in order to modify electrochemical sensors, therefore, the combination of PB, CNTs and metal nanoparticles have received special attention. You *et al.* [7] reported the electrocatalytic reduction of hydrogen peroxide using carbon nanotubes and Pd nanoparticles. The electrode showed a good linear detection range which is attributed to the improved sensitivity and selectivity given by the combination of Pd and CNTs.[7] Carbon nanotubes have good electric conductivity, therefore they can be used as a mediator for PB-modified electrodes. For instance, Wang *et al.* [8] reported the determination of hydrogen peroxide on an electrode based on Prussian blue and CNTs. Electrochemical sensors for hydrogen peroxide (H_2O_2) detection are developed by adding electroactive materials (metals, metal oxides, enzymes, etc.) on the surface of electrodes. Hydrogen peroxide is a mediator found in the majority of biological reactions.

Considering all those facts, in this work, the carbon nanotubes (CNTs) and zirconia doped carbon nanotubes (ZrO_2 -CNTs) were used for electrode modification.

I.I Problem Statement

Carbon nanotubes (CNTs) have been used to fabricate sensors and biosensors because of their unique structure, electronic, mechanical and biocompatible properties. However, great efforts have been made to obtain excellent electrochemical properties, such as high reactive areas and optimum surface area. Moreover, enzyme based biosensors are quite difficult to develop and even more to avoid enzyme denaturalization.

Based on those observations, the present work proposed the development of metal oxide doped carbon nanotubes and an inorganic compound as an electrocatalyst.

I.II General Objectives

Develop a sensor based on Prussian blue (PB) deposited electrochemically on a glassy carbon electrode modified drop-casting with carbon nanotubes (CNTs) and zirconia doped carbon nanotubes (ZrO_2 -CNTs), in order to perform electrochemical detection of hydrogen peroxide (H_2O_2).

I.III Specific Objectives

- Characterize pristine carbon nanotubes, functionalized carbon nanotubes and zirconia doped carbon nanotubes.
- Modify a glassy carbon electrode with the functionalized carbon nanotubes and zirconia doped carbon nanotubes.
- Electrochemical characterization of the modified electrodes.
- Evaluate and quantify the electrochemical response of the modified electrodes in hydrogen peroxide solutions.

Chapter 1

Theoretical background

1.1 Biosensors

A biosensor is a complex sensing device which consists of a bio-recognition element and a transducer. The main part of the biosensor is the bio-recognition system which allows a selective detection, and it will identify and interact with the analyte and its physicochemical changes. Then, the physicochemical changes in the analyte are converted into electrical signal by the transducer.[2] Another important aspect of biosensors is its versatility, then it is an interdisciplinary technology which involves engineering, physics, chemistry, biotechnology, biology, and others.[9] The classification of biosensors is based on the type of bio-recognition element or the transducing method used. Typical bio-recognition elements used are enzymes, antibodies, tissues, microorganisms, and among others. For instance, there are antibody-based biosensors, enzyme-based biosensor, cell-based biosensors, acid-based biosensors (DNA biosensors), etc. As for different transducing methods, the biosensors are classified as piezoelectric, optical, or electrochemical biosensors.[2] Most of the developed biosensors are electrochemical and enzyme-based biosensors due to their high sensitivity, simple operation and less expenditure, furthermore they can be applied to the rapid detection of the molecules of interest. In addition, enzyme sensors and electrochemical sensors can be modified to show high sensitivity and selectivity.[10] Recent development in biosensors are focused on producing small and portable devices that would allow fast and accurate detection, therefore nanostructure based biosensors are very promising.[2]

1.2 Hydrogen peroxide

Hydrogen peroxide (H_2O_2) is an essential mediator used in many fields, especially, in the field of environmental analysis and in industries. [4] In fact, H_2O_2 as a universal oxidant agent has wide applications in industrial processes, and it is an important intermediate agent in environmental and biological reactions. Therefore, the study on H_2O_2 determination is significant for both industrial and academic purposes. The determination of H_2O_2 has been important over the past century, and this is still something to accomplish in order to find an accurate, effective and rapid technique. Many techniques including titrimetry, spectrometry, and chemiluminescence have been employed for the determination of hydrogen peroxide.[4] These methods are of high sensitivity and selectivity. However, they are expensive, time consuming, etc., among other drawbacks. Fortunately, electrochemical sensors can overcome the above mentioned difficulties due to their good performance characteristics, including high sensitivity, rapid detection simplicity, and portability.

A large range of materials such as redox proteins, transition metals, metal oxides, metal phthalocyanines and redox polymers have been employed to conduct electrocatalytic hydrogen peroxide detection. On the other hand, recent advances in nanomaterials have attracted interest because of their chemical, physical and electronic properties which are different from those of bulk materials. Moreover, the nanomaterials can be tuned for designing a sensing platform and enhancing sensing performance by controlling their size and structure.[11]

1.3 Metal hexacyanoferrates: ferric hexacyanoferrate

Ferric hexacyanoferrate $\text{Fe}_4^{\text{III}}[\text{Fe}^{\text{II}}(\text{CN})_6]_3$ or Prussian blue (PB) is considered as an artificial peroxidase. The catalytic capability is due to the reduced form of PB called Prussian white (PW). The catalyzing process of the reduction of H_2O_2 occurs at low potentials.[12] The synthesis of Prussian blue can be achieved by mixing ferric and hexacyanoferrate ions with different oxidation state of iron atoms. The following combinations of ions are most used: $\text{Fe}^{3+} + [\text{Fe}^{\text{II}}(\text{CN})_6]^{4-}$ or $\text{Fe}^{2+} + [\text{Fe}^{\text{III}}(\text{CN})_6]^{3-}$. Herren *et al.* [13] studied the crystalline structure of PB by electron and neutron diffraction measurements, they reported that PB has a cubic structure consisting of alternating Fe(II) and Fe(III) placed on a face centered cubic lattice. In this structure, Fe(III) ions are surrounded octahedrally by nitrogen atoms, and Fe(II) ions are surrounded by carbon atoms. The cubic unit cell dimensions are 10.2 Å.[13] The good catalytic specificity to hydrogen peroxide is due to the polycrystalline structure of PB which presumably allow penetration of only small molecules into its lattice structure. Therefore, Prussian blue-based electrodes have been studied and used in biosensor construction. Additionally, the advances in nanotechnology have been used to

develop sensors based in nanomaterials.

Sheng *et al.* [6] report a synthesis of hollow PB (HPB) structure as a highly sensitive electrochemical sensor for the determination of H_2O_2 . They found that the sensor based on HPB, chitosan (CS) and GC electrode exhibits enhanced performance in the electrocatalytic activity for reduction of H_2O_2 with a good linear response, high sensitivity ($693.0 \mu\text{A mM}^{-1} \text{cm}^{-2}$), a wide detection range (8-1848 μM) and a low detection limit (2.6 μM). [6] Other studies involve the combination of nanomaterials with high sensitivity and selectivity, for instance, Ge *et al.* [14] fabricated Prussian blue nanocube on graphene oxide (PBNCs/GO) and studied the electrochemical sensing of hydrogen peroxide using a PBNCs/GO modified gold electrode. The PBNCs/GO modified Au electrode showed a good linear range detection of 0.002 - 2.8 mM with a detection limit of 0.48 μM , and a sensitivity of $2502 \mu\text{A mM}^{-1} \text{cm}^{-2}$. [14] The prominent electrocatalytic activity for reduction of H_2O_2 is attributed to the synergistic effect of the GO and PBNCs. Zhang *et al.* [5] developed an electrode platform for enzyme loading by coupling nitrogen doped graphite foam (NGF) with PB particles. The PB/NGF electrode was used to quantify H_2O_2 , the electrode showed a linear range of 0.004 to 1.6 mM with 2.4 μM as a detection limit. [5] They also immobilized glucose oxidase (GOx) in the electrode by the cross-linking method, and develop the GOx/PB/NGF biosensor which was used to detect glucose in human serum. [5] This electrode responded to glucose over the 0.2 to 20 mM concentration range, with a sensitivity of $27.48 \text{ mA M}^{-1} \text{cm}^{-2}$, and 0.1 M detection limit. [5] They suggest that the PB/NGF electrode can serve as a supporter for other enzymes, which holds a promise for biosensing applications.

1.4 Zirconium dioxide

Zirconium dioxide (ZrO_2) also referred as zirconia is an inorganic metal oxide used in the field of ceramic materials. In nature, zirconia is found in its mineral form with a crystalline monoclinic structure which is called baddeleyite. [15] Zirconium dioxide depending on the temperature of synthesis exhibits three crystalline structures which are monoclinic, tetragonal, and cubic. Monoclinic structure is stable at temperatures below 1170°C , the tetragonal structure is stable at temperatures between $1170 - 2370^\circ\text{C}$, and the cubic structure stability is at temperatures in the range of 2370 to 2680°C . [16] Zirconium dioxide have been used in the ceramics field due to its high hardness and high melting point.

1.5 Carbon nanotubes

Carbon in nature exists in many molecular forms which are called allotropes. Graphite, diamond, fullerenes, amorphous carbon, carbon nanotubes, etc., are allotropes of carbon, each one has different and unique properties. One of the interesting allotropes is the CNT which exhibits excellent thermal conductivity, high surface area, high mechanical strength, good chemical stability, fast electron transfer rate, among others.[17] CNTs are the result of rolling up one or more graphene layers in a tube-like structure obtaining a cylindrical shape. Electronic properties of CNTs depend on the structure of the tube. Based on the way graphene layers are rolled up, the structure of nanotubes can be an armchair, chiral or zigzag which correspond to metallic or semiconducting behavior.[18] According to the number of graphene layers rolled up, nanotubes are classified into two groups, single-wall carbon nanotube (SWCNT) which are made of a single layer of graphene, and multiwall carbon nanotubes (MWCNTs) composed of several layers of graphene.[18] The layers in a MWCNTs are separated 0.34 nm, and they have an outer diameter of about 10-50 nm.[19] Chemical bonding found in CNTs is the sp^2 bond which are stronger than the sp^3 bonding, then it provides the unique strength to nanotubes.[1] A disadvantage found in nanotubes is their high hydrophobicity and chemical inertness.[20] Thus, CNTs are modified chemically or functionalized in order to be used for different purposes.

1.5.1 Functionalization of carbon nanotubes

There are several methods and approaches of functionalization taking advantages the structural defects. The aim of the functionalization of CNT is to solubilize the nanotubes by attaching hydrophilic species to the surface of tubes. The poor solubility is due to the strong $\pi-\pi$ interaction of the nanotube.[21] The methods of functionalization can be divided into two large groups which are the covalent and non-covalent functionalization. Covalent functionalization forms new covalent bonds between the carbon atoms of the nanotube and the atoms of the molecule, then it produces strong and stable attachments of functional groups to CNT. On the other hand, non-covalent functionalization involves the adsorption of molecules to the surface of nanotubes forming a chemical bond (i.e. van der Waals) or wrapping molecules helically around the nanotube.

1.5.1.1 Non-covalent functionalization

In this type of functionalization, the CNTs are not modified structurally, it means the original structure is retained. Although, the stability is lower compared to covalent functionalization. The chemical interactions generated between

the molecules and nanotubes are weak. These interactions are usually the van der Waals forces and interaction of the $\pi - \pi$ stacking. For instance, electrostatic interactions are used for functionalizing nanotubes with biomolecules. Electrochemical biosensors utilize the electrostatic stabilization of layers to form a compact and stable system.[22] For this type of functionalization, special equipment is not necessary, therefore this method is scalable for future applications.

There are three main types of molecules used for non-covalent functionalization which are the small aromatic molecules, biomolecules, and polymers. Commonly, the molecules are attached to the CNTs using $\pi - \pi$ interactions, especially for small aromatic molecules such as cyclohexane.

Small aromatic molecules and surfactants non-covalently functionalize the CNTs through $\pi - \pi$ stacking and hydrophobic interactions. For instance, Chen *et al.* [23] reported an immobilization of proteins on the CNTs using bifunctional molecules. The immobilized proteins were observed with atomic force microscopy (AFM) and transmission electron microscopy (TEM). They conclude that the non-covalent functionalization method used is efficient for immobilization of biomolecules.[23]

Furthermore, polymers and copolymers can be used to noncovalent functionalization of CNTs. Wrapping polymers helically in a nanotube is a result of the formation of $\pi - \pi$ interactions and van der Waals interactions between polymers and the surface of the CNTs.[24] Zhan *et al.* [25] reported non-covalently attached polymers onto the surface of MWCNTs through hydrophobic interactions and electrostatic attractions. They obtained a polymer-based nanocomposite which shows good biocompatibility for protein immobilization, and as a biosensor showed a fast response and excellent linear range detection.[25]

Major applications of the non-covalent CNT functionalization is the use of surfactant molecules to stabilize individual CNTs in an aqueous medium, furthermore, non-covalently functionalized nanotubes are widely used for drug delivery, imaging and sensors in the field of biochemistry and medicine.[23],[25]

1.5.1.2 Covalent functionalization

The covalent functionalization is a chemical modification which create covalent bonds between the CNT and the modifier species. The wide diversity of functions obtained, together with the high stability of the nanomaterials chemically functionalized are some of the greatest advantages of covalent functionalization.[26] There is not a systematic classification of the types of covalent functionalization, however, the criteria used in most reports is based on the anchoring sites of functional groups on the CNTs. Therefore, there are two main methods of covalent functionalization which are the defect-group functionalization, and direct covalent termini or sidewall functionalization.[27]

The strong and stable anchoring of functional groups allows application of CNTs in a harsh environmental conditions and might be used for *in vivo* studies. Wang and Swager [28] report a covalently functionalized MWCNTs-based sensor to detect and provide a clear classification of volatile organic compounds based on functional group identification. The functional groups anchored on MWCNT surfaces enhance greatly sensitivity and selectivity on the targeted analytes. Furthermore, they found that the sensor is promising for detection and identification of other volatile organic compounds present in nature due to contamination.[28]

Most of the studies related to covalent functionalization of CNTs are focused to enhance the selectivity and sensitivity of nanotubes to small molecules. Huang *et al.* [29] reported double-wall carbon nanotube (DWCNT) covalently functionalized to enhance the sensitivity and selectivity. They found that the device based on DWCNTs shows excellent detection properties and selectivity. The device was able to detect until the amount of 60 nM of HN_3 and simultaneously displaying a high chemical selectivity toward a variety of amine-containing analyte molecules over other small molecule analytes.[29] The covalently functionalized CNTs open new opportunities for chemical and biological sensing, and in this cases, the high sensitivity and selectivity are useful to detect trace elements.

Summarizing, non-covalent functionalization preserves generally the intrinsic properties of CNTs, therefore full properties are retained. However, for applications in medical and environmental fields, CNTs covalently functionalized are more stable. One of the advancement in covalent functionalization is the synthesis routes that carry out several stages. It consists of a primary functionalization in order to make CNTs more reactive, later a second functionalization is performed. Usually, the second functionalization anchor complex molecules to the previous functionalization.[21]

1.6 Nanostructured composite materials

Nanostructured materials are nanomaterials formed by two or three different nanomaterials, the objective of these materials is to obtain improved properties compared to the raw materials used. Nanostructured materials are widely studied in order to enhance properties and find new applications.[30]

1.6.1 Nanostructured materials composed of CNTs and metal oxides

In the last years, the influence of metal oxides on nanomaterials (CNTs, graphene, NPs) has been studied in order to develop nanomaterials with improved properties. For instance, Kayvani Fard *et al.* [31] synthesize ferric oxide doped carbon nanotubes for adsorption applications. Ma and Tian [32] used the MWCNTs coated with the zinc

oxide (ZnO) to studied its electron transfer and electrocatalysis of hemoglobin (Hb).

Nanostructured materials can be synthesized by different methods, such as sol-gel, electro-spinning and chemical vapor deposition. The most used method is the sol-gel method due to its simplicity.

1.6.2 Sol-gel method

Sol-gel method is mostly used in the synthesis of nanostructure materials, then it was used to synthesize the ZrO_2 -CNTs.

The sol-gel method is based on hydrolysis reactions (eq. 1.1) and condensation of the precursor (eq. 1.2). The sol is a stable suspension of colloidal solid particle or polymers in a liquid, and gel is a porous, three dimensional, continuous solid network surrounding a continuous liquid phase. The synthesis of metal oxides is achieved through metal alkoxides as the precursors.[30] In this method, acid catalysts are used to control the velocity of hydrolysis, also it controls the formation of nanometric particles.[33]



M is the metal ion and **R** is the alkyl group

1.7 Carbon nanotubes based electrochemical biosensors

Nanotechnology has provided novel nanomaterials to enhance most of the properties of bulk materials through synergistic effects or combining properties. Many nanomaterials have been used for different purposes in the field of biosensors, for instance, they are used to immobilize molecules on the surface of electrodes, other nanomaterials are used to enhance the electron-transfer rate, or only as working electrodes which utilize their large specific surface area. CNT-based biosensors are widely studied as well as their combination with other composites.

Previous studies about CNTs are related to changes of electrochemical properties of nanotubes by modifying them with other nanomaterials. Ma and Tian [32] studied the electron transfer and electrocatalysis of Hb in MWCNTs coated with the zinc oxide (ZnO). They report that Hb shown high electroactivity and electrocatalytic response to H_2O_2 . Furthermore, the nanostructure composite demonstrated to be suitable for the immobilization of Hb, and satisfactory reproducibility and high stability.[32] They report the direct electron transfer was achieved getting a synergic effect between ZnO coated MWCNTs and the surface of the glassy carbon electrode.

As in the research of Ma and Tian [32] the use of other nanomaterial to enhance properties of CNTs is widely study, similarly, Zhao *et al.* [34] reported the bioelectrocatalytic activity of CNTs-hydroxyapatite-hemoglobin nanocomposite. The hydroxyapatite (HA) was used to improve the bioactivity and biocompatibility of the composite. They demonstrated that the MWCNTs-HA nanocomposite provide a favorable matrix to immobilize Hb, moreover, they used this nanocomposite as a hydrogen peroxide biosensor which showed fast amperometric response, high reproducibility and stability.[34] These results suggest that CNTs can be used in the field of bioelectronic devices such as, electrochemical biosensors for biomolecule sensing applications.

According to previous studies modified CNTs can be used for sensing purposes. For instance, Hobbs *et al.* [35] reported a fabrication of CNTs-based enzyme-modified biosensor electrode, and glucose determination. The results suggest that the CNTs-based biosensor with a glucose oxidase enzyme immobilized were able to detect glucose in beverage. The amount of glucose found was 0.253 ± 0.053 M in a Sprite drink.[35] CNTs used in this research were not modified with any other nanomaterial. Wei *et al.* [36] reported the detection of pesticide residues using a MWCNTs-titanium oxide with caboxymethyl chitosan modified electrode. The results indicate that the nanocomposite modified electrode could be used to detect pesticide residues, moreover, they were able to detect trichlorfon residues in food. Nanocomposite modified electrode shown a wide linear range and low detection limit.[36]

1.8 Experimental techniques

1.8.1 Transmission electron microscopy (TEM)

TEM is a technique used to observe nanometric materials. TEM gives information about the morphology of the sample, crystalline structure and chemical composition. TEM is composed mainly by an electron source, a sample holder, a system of objective lenses, a setup of magnifying lenses and data collector. The main advantages of TEM are images of high resolution, electron diffraction analysis, and elemental microanalysis when the equipment has an energy dispersive spectroscopy (EDS) spectrometer.

1.8.2 Fourier transform infrared (FTIR) spectroscopy

Fourier transform infrared (FTIR) spectroscopy is a technique utilized to identify functional groups and organic substances, also it can be used to determine the relative concentration of certain substances in a mixture of them. FTIR is based on the vibrational and rotational modes of a molecule when this is exposed to infrared radiation.[37] Typically, a FTIR spectrum is between 400 to 4000 cm^{-1} . The functional groups' region is in the range from 1200 to

4000 cm^{-1} because of the presence of the bands associated to the individual bond vibrations and functional groups, while the bands below the 1200 cm^{-1} are called fingerprint due to each molecule has characteristic bands in this region.[37]

1.8.3 X-ray diffraction (XRD)

X-ray diffraction (XRD) is a powerful technique to study the crystalline structure of materials. It gives structure, phase, crystallinity, crystal defects and size information related to the material. X-ray diffraction is a technique based on the constructive interference of electromagnetic radiation (monochromatic X-rays) of a certain energy level and a crystalline sample. [38] When Bragg's law (eq. 1.3) is satisfied by the incident rays, it produces constructive interference and diffracted rays, then it generates a diffraction pattern showing intensity as a function of incident angle.

$$n \lambda = 2 d \sin \theta \quad (1.3)$$

In equation 1.3, n is an integer number, λ is a wavelength of the x-ray, d is the interplanar spacing generating the diffraction, and the θ is the diffraction angle.

Moreover, the crystal size can be obtained using the Scherrer's equation (eq.1.4) which relates the full width at half maximum (FWHM) of the main peak to its diffraction angle.

$$D = \frac{0.89 \lambda}{\beta \cos \theta} \quad (1.4)$$

Where D is the diameter of the crystal, λ is the wavelength of $\text{CuK}\alpha$ radiation, θ is the Bragg diffraction angle and β is the corrected width peak and equal to: $\beta = \sqrt{B^2 - b^2}$, B is the observed peak width, and b is the instrumental broadening.

1.8.4 Cyclic voltammetry (CV)

Cyclic voltammetry (CV) is a powerful tool to monitor reactions involving electron transfer. Cyclic voltammetry is a popular electrochemistry technique commonly employed to investigate the reduction and oxidation process of molecular species. This technique provides qualitative information about electrochemical reactions, such as the thermodynamics of redox processes, the kinetics of reactions by electron transfer or adsorption, etc. The power of this technique results from its capability for rapidly placing the redox potentials of the electroactive species, as well

evaluation of the effect of the medium of such processes. [39] This technique consists of applying a linear sweep of potential in a working electrode using a potential in a triangular form (Figure 1.1a). During the potential sweep, measurements of the generated current are made according to the applied potential. The spectra obtained from the CV experiment are called cyclic voltammograms (Figure 1.1b), the abscissa represents the applied potential respect to reference electrode and the ordinate is the current. There are two conventions used to report cyclic voltammograms, which are US convention and IUPAC convention.[40] The results showed in this document are based on IUPAC convention.

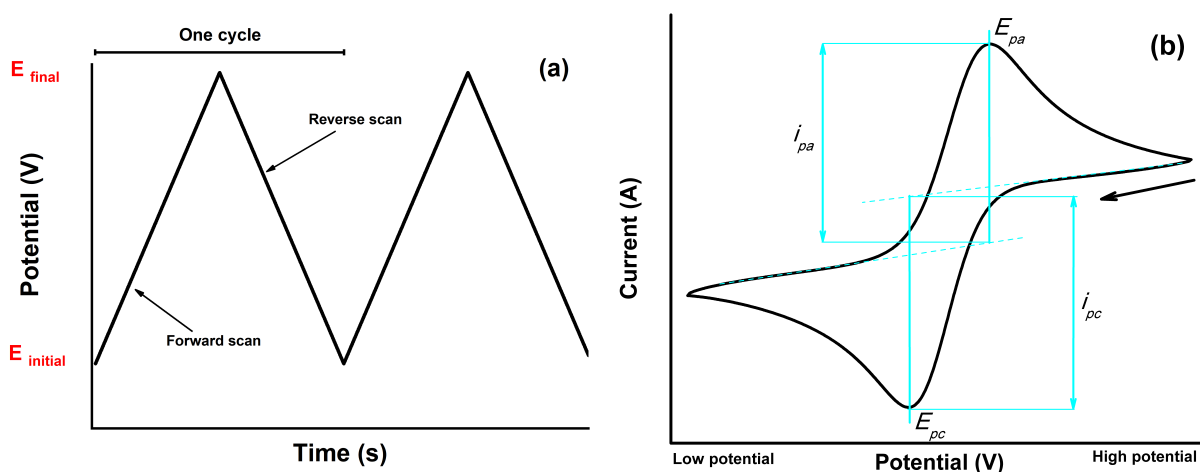


Figure 1.1: Cyclic voltammetry responses diagrams (a) Waveform for cyclic voltammetry. (b) Cyclic voltammogram of reversible redox process at a given scan rate (ν).

Figure 1.1b illustrates the response of a reversible redox pair (eq. 1.5) during a simple potential scan cycle. As the potential is scanned in the negative direction the current decays (reduction peak: i_{pc}) and then rise to a peak (oxidation peak: i_{pa}). The characteristic peaks of a cyclic voltammogram are due to the formation of a diffusion layer near to the surface of the working electrode electrode. CV allows to determine the type of redox process, for instance, it can be electrochemically reversible, quasi-reversible or irreversible.



Among the important parameters, scan rate is a crucial parameter. Briefly, the scan rate is the linear change of the potential in time. The faster the scan rates, the higher the current obtained. A fast scan rate decreases the size of the

diffusion layer, then the current observed is high. [41] The cyclic voltammograms are useful to calculate parameters such as: the formal peak potential ($E^{\circ'}$), peak-to-peak separation (ΔE_p), anodic peak current (i_{pa}) and cathodic peak current (i_{pc}), ratio of redox peak current (i_{pa}/i_{pc}), and the electrochemical area (A) of the electrode.

1.8.4.1 Reversible systems

A reversible system is that in which it is possible to oxidize the species R through a sweep in the anodic direction and with a reverse scan return to species R to its oxidized state. Quantitatively, in a reversible system the difference between the anodic and cathodic peak potential, called peak-to-peak separation (ΔE_p) (eq. 1.6), is 59 mV at 25°C. [41]

$$\Delta E_p = E_{pa} - E_{pc} \quad (1.6)$$

For a process of this type, the peak current is given by the equation of Randles-Sevcik (eq 1.7). Additionally, the Randles-Sevcik equation describes a linear relationship of the the peak current (i_p) with respect to root square of scan rate ($\nu^{1/2}$), where i_p is the current (A), n is the number of electrons transferred in the redox event, A is the geometric area of the electrode (cm^2), D_o is the diffusion coefficient of the analyte ($\text{cm}^2 \text{ s}^{-1}$), and C° is the bulk concentration of the analyte (mol cm^{-3}).

$$i_p = 2.69 \times 10^5 n^{3/2} A C^\circ D_o^{1/2} \nu^{1/2} \quad (1.7)$$

The position of peaks on the potential is related with the $E^{\circ'}$ of the redox process. The formal peak potential for a set of reversible system is centered between anodic peak potential (E_{pa}) and cathodic peak potential (E_{pc}) (eq. 1.8).

$$E^{\circ'} = \frac{E_{pa} + E_{pc}}{2} \quad (1.8)$$

The equations stated above (eq. 1.6, 1.7, 1.8) are very useful to study the electrochemical reversible electron transfer processes involving freely diffusing redox species. For instance, the deviation in the linear relationship in the plot of i_p vs. $\nu^{1/2}$ might be related to an electrochemical quasi-reversibility or surface-adsorbed electron transfer. An accurate detection of the cause of the linear deviation is acquired by measuring the formal potential and peak-to-peak separation potential. A quasi-reversible process is related to the shift of peak-to-peak separation potential while a no peak-to-peak separation potential is associated with a surface-adsorbed species.[40]

1.8.4.2 Quasi-reversible and irreversible systems

The quasi-reversible system is a redox process controlled by the charge transfer and mass transport. The cyclic voltammograms of a quasi-reversible system are elongated and exhibit a large separation of peak potentials compared

to those of a reversible system.

A irreversible system shows a cyclic voltammogram with size reduced peak and a wide separation. A totally irreversible system exhibits a change in the peak potential with the scan rate.[41]

1.8.5 Chronoamperometry (CA)

The chronoamperometry (CA) involves potential pulses over the working electrode from a value where no-faradic process occurs to a potential where the surface concentration of the electroactive species is effectively zero. In CA technique, the current decays with time (Figure 1.2b), this relationship is given by the Cottrell equation (eq. 1.9). When $i t^{1/2}$ is constant, this state is called Cottrell behavior.[41]

$$i = \frac{n F A C^{\circ} D_o^{1/2}}{\pi^{1/2} t^{1/2}} \quad (1.9)$$

Where i is the current (A), n is the number of electrons transferred, F is the Faraday constant, 96485 C/mol, A is the electrode surface area (cm²), D_o is the diffusion coefficient of the analyte (cm² s⁻¹), t is the time (s), and C° initial concentration of the reducible analyte (mol cm⁻³).

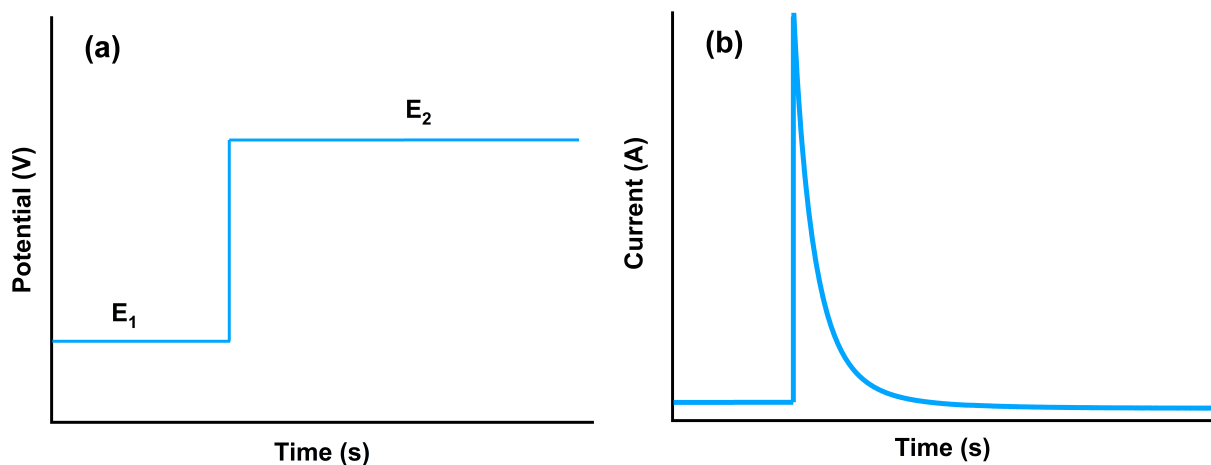


Figure 1.2: Chronoamperometry response diagrams (a) potential-time response; (b) current-time response

Chapter 2

Methodology

This section provides a description of reagents, preparation of solutions, modification of electrodes and conditions of experiments, also the equipment used to achieve the objectives established. The reagents used are described with their degree of purity.

2.1 Reagents and solutions

All solutions were prepared with distilled water (DI). Carbon nanotubes (CNTs) were obtained from Material Science & Nanotechnology Laboratory (IVIC, Caracas, Venezuela), potassium phosphate monobasic (KH_2PO_4), sodium hydroxide (NaOH), nitric acid (HNO_3) (Fisher Chemical A200C-212, 69.2%), potassium ferricyanide ($\text{K}_3[\text{Fe}(\text{CN})_6]$), ferric chloride hexahydrated ($\text{FeCl}_3 \cdot 6\text{H}_2\text{O}$), hydrochloric acid (HCl, 37%), potassium chloride (KCl), sodium chloride (NaCl), hydrogen peroxide (H_2O_2) (30% w/w in H_2O), *N,N*-Dimethylformamide (DMF) and poly(diallyldimethylammonium chloride) (PDDA)(35 wt% in H_2O).

2.1.1 Carbon nanotubes (CNTs) suspension

Functionalized carbon nanotubes (CNT-COOH) and zirconia doped carbon nanotubes (ZrO_2 -CNTs) were suspended in DMF at a concentration of 5.0 mg/mL, then these suspensions were sonicated about 15 min, and stored at room temperature and sealed with parafilm.

2.1.2 Poly(diallyldimethylammonium chloride) (PDDA) solution

PDDA is a positively charged ionic polymer. The solution of PDDA was prepared in 0.5 M NaCl at a concentration of 1 mg/mL. PDDA is used to achieve an electrostatic stability between the modifier layers.[35]

2.1.3 Phosphate buffer saline (PBS) solution

The electrolyte solution used for all experiments was the 0.1 M phosphate buffer saline (PBS) solution at pH 7.0. PBS was prepared with 250 mL of 0.01 M of KH_2PO_4 , then it was mixed with 73 mL of 0.2 M of NaOH, finally, distilled water was added until it reach 500 mL.

2.2 Functionalization of carbon nanotubes

The functionalization of carbon nanotubes and nanostructured materials were carried out in a previous work by Y. Sarmiento [42]. The functionalization was made in two parts the prefunctionalization and functionalization.

2.2.1 Prefunctionalization of carbon nanotubes (CNTs)

The prefunctionalization procedure followed by Sarmiento [42] is described below.

1.0 g of CNTs were added in a 500 mL volumetric flask, then 100 mL of 3.0 M of nitric acid and 300 mL of 1.0 M of sulphuric acid were added in this order.

The reaction mixture was placed under a reflux at a temperature of about 80 °C and a stirring speed of 400 rpm for six hours.

Once the mixture was cooled to room temperature, CNTs were filtered in a porous frit plate, and washed with deionized water until the wash solution reached a neutral pH.

Afterwards, the washed CNTs were dried in an oven under low vacuum at 25 inches of Hg and 60 °C for 12 h, finally CNTs were ground in a mortar.

2.2.2 Functionalization of carbon nanotubes (CNTs)

To add carboxylic ($-\text{COOH}$) and hydroxyl ($-\text{OH}$) groups to the side-wall of CNTs the following procedures were performed.

80 mL solution of nitric acid 60 wt% were added in a 250 mL volumetric flask with prefunctionalized CNTs. The mixture was placed under ultrasonic agitation for 30 min and then under reflux at 80 °C and 400 rpm for two hours. Then, the mixture was cooled at room temperature and diluted with 200 mL of deionized water, next, the filtering process was made as described in prefunctionalization section.

Subsequently, CNTs were dried in an oven under low vacuum at 25 inches of Hg and 60 °C for 16 h, finally CNTs were grounded in a mortar and then sieved using a 125 µm sieve.

2.2.3 Synthesis of ZrO₂-CNT nanostructured system

The ZrO₂ was synthesized *in situ* on the functionalized CNTs by sol-gel method. The synthesis was described in a previous work by Sarmiento [42].

2.2.3.1 Reagents and amount of reagents

The amount of reagents used belong to the synthesis of ZrO₂-CNTs 36% by weight of CNTs with respect to the zirconia.

- 0.08 g of functionalized CNTs
- 0.60 mL of zirconia propoxide
- 5.70 mL of propanol
- 0.13 mL of deionized water
- 0.60 mL of acetic acid

2.2.3.2 Procedure

Half volume of propanol was added to a volumetric flask with CNTs, then it was subjected to ultrasonic agitation. Then, zirconia propoxide, 1/4 volume of propanol, and acetic acid were added to other volumetric flask, and this mixture was subjected to ultrasonic agitation for 10 min.

Afterwards, the above mixture was placed in an addition vessel to drop it on the propanol and CNTs solution, which was subjected to mechanical agitation at 600 rpm at room temperature.

Next, a propanol in deionized water solution was added drop by drop to the previous mixture.

After adding the reagents, the reaction was maintained for two hours, and allowed to age 20 days.

After aging time, the mixture was placed in a beaker, washing the volumetric flask with alcohol. The solvent was evaporated at about 88 °C until a pasty mixture was obtained. Then, deionized water, three times the volume of the mixture, was added to the pasty mixture, which were evaporated at temperature between 88 - 96 °C.

Subsequently, the resulting substance was dried in low vacuum at 80 °C for 4 h, afterwards, a thermal treatment was performed in argon atmosphere at 50 °C for 2 h.

Finally, the sample was grounded in a mortar.

2.3 Physical and morphological characterization conditions

2.3.1 Transmission electron microscopy (TEM)

Transmission electron microscopy (TEM) images were taken in a JEOL 1220 microscope at an acceleration voltage of 100 kV and 200 kV. The samples were suspended by adding 3.0 mL of ethanol/water 70% in a vial with a tiny amount of sample. This suspension was sonicated for 10 minutes, and a drop of this suspension was placed in TEM mesh.

2.3.2 X-ray diffraction (XRD)

The crystalline structure and phase of the CNTs and ZrO₂-CNTs are studied by x-ray diffraction (XRD). XRD spectrum of samples was registered by SIMENS D5005 diffractometer, at a wavelength (λ) of 1.54178 Å. The samples were analyzed in the range of $2\theta = 10^\circ - 80^\circ$ at a scan rate of 0.02°/0.52s.

2.3.3 Fourier transform infrared (FTIR) spectroscopy

The presence of functional groups or organic compounds in the nanotubes and ZrO₂-CNTs are studied by fourier transform infraed (FTIR). FTIR spectrum were recorded in a Nicolet iS10 FTIR spectrometer. Samples in powder form were evaluated in KBr pellets with a concentration of 0.2 to 1% in the pellet.

2.4 Electrochemistry

All electrochemical experiments were performed on a CHI 1230 C Handheld Potentiostat (CH Instruments, Inc.) with a conventional three-electrode system. The bare glassy carbon (GC) and modified electrodes were used as

working electrode, a graphite rod as the counter electrode, and a commercial Ag/AgCl electrode (3.0 M KCl) as the reference electrode. The supporting electrolyte used was the 0.1 M PBS at pH 7.0. The electron transfer behavior of the working electrodes was studied with 4.0 mM of $K_3[Fe(CN)_6]$ in 0.1 M PBS at pH 7.0 by performing cyclic voltammetry technique at different scan rate (ν). All measurements were performed at room temperature, and all potentials are reported against the Ag/AgCl reference electrode.

2.4.1 Analytic characterization

2.4.1.1 Geometric area

It can be calculated from the slope of the calibration curve of current against square root of scan rate ($\nu^{1/2}$) and by the use of the Randles-Sevcik (eq. 1.7). The bulk concentration (C°) was 4×10^{-6} mol cm^{-3} and the diffusion coefficient (D_o) of the ferricyanide ($[Fe(CN)_6^{3-}]$) used was 7.35×10^{-6} cm^2/s . [9]

2.4.1.2 Double layer capacitance

The double layer capacitance (C_{dl}) can be calculated using the equation 2.1.

$$i_c = A C_{dl} \nu \quad (2.1)$$

Where i_c (A) is the charging current, A (cm^2) is the geometric area of the electrode, ν (V/s) is the scan rate, and C_{dl} (F/ cm^2) is the double layer capacitance.

2.4.1.3 Sensitivity

The maximum peak current is recorded at different concentrations of H_2O_2 , and the slope of the calibration curve corresponds to the sensitivity of the sensor. [43]

2.4.1.4 Limit of detection (LOD)

Limit of detection (LOD) is defined as the minimum amount of substance, for example H_2O_2 , that can be detected but not necessarily quantified. [43] Limit of detection can be calculated by the equation 2.2.

$$LOD = 3 \frac{\sigma}{m} \quad (2.2)$$

Where σ is the standard deviation of the net concentration when the analyte is not present in the sample, and m is the slope of the calibration curve.

2.5 Preparation of modified electrodes

Prior to modification, GC electrode ($\Phi = 3$ mm, CHI104) was polished successively with 1.0 μm , 0.3 μm and 0.05 μm alumina slurry on a polishing cloth pad until mirror like surface, and rinsed with distilled water (DI). Afterwards, the electrode was polished electrochemically by cyclic voltammetry at a potential between -1.6 to 1.9 V at 100 mV/s in 0.1 M HNO_3 solution for 25 cycles. Before each experiment the GC electrode was cleaned with this procedure.

2.5.1 Preparation of carbon nanotubes (CNTs) modified electrodes

A volume of 10 μL of CNTs suspension was pipetted on the surface of GC electrode. The GC electrode was allowed to dry during 15 min at 50 $^\circ\text{C}$, after that 10 μL of the PDDA solution was pipetted on the modified GC electrode, and dry during 15 min at 50 $^\circ\text{C}$. The modified electrode (PDDA/CNTs/GC) was rinsed with distilled water and stored at room temperature.

The PDDA/ ZrO_2 -CNTs/GC electrode was prepared also by this procedure and stored at room temperature.

2.5.2 Preparation of Prussian blue (PB) based electrodes

Prussian blue (PB) is an excellent catalyst for H_2O_2 reduction at moderate potentials, also, it emulates peroxidase enzyme. Once the GC electrode was modified with CNTs and ZrO_2 -CNTs, the PB was electrodeposited as follows.[44] Electrodeposition of PB was accomplished in an aqueous solution containing 2.5 mM $\text{K}_3[\text{Fe}(\text{CN})_6]$ + 2.5 mM $\text{FeCl}_3 \cdot 6\text{H}_2\text{O}$ + 0.1 M KCl + 0.1 M HCl at potential of $+0.4$ V during 60 s for two steps (See table 2.1).

Table 2.1: Chronoamperometric parameters for electrodeposition of PB

Initial potential (V)	0
High potential (V)	0.4
Low potential (V)	0
Initial scan direction	Positive
Step	2
Pulse width (s)	60
Sample interval (s)	0.001
Quiet time	5
Sensitivity(A/V)	0.001

Subsequently, the PB electrodeposited electrode was activated by cycling at a potential range from -0.05 to 0.35 V at 50 mV/s in 0.1 M KCl + 0.1 M HCl solution for 20 cycles (See table 2.2). Every solution was purged with N₂. The PB based electrodes were allowed to dry at 50 °C during 15 min, finally, a volume of 10 µL of PDDA solution was cast on the modified electrode and allowed to dry during 15 min at 50 °C. The modified GC electrodes were stored at room temperature.

Table 2.2: Cyclic voltammetry parameters for stability evaluation of electrodeposited PB

Initial potential (V)	0.35
High potential (V)	0.35
Low potential (V)	-0.05
Initial scan direction	Negative
Scan rate (V/s)	0.05
Segment	40
Sample interval (s)	0.001
Quiet time	5
Sensitivity(A/V)	0.001

2.6 Hydrogen peroxide (H₂O₂) determination conditions

A stock solution of 0.1 M hydrogen peroxide (H₂O₂) was prepared in distilled water, from this stock solution the H₂O₂ concentration of 0.5, 1.0, 1.5, 2.0, 2.5, 3.0, 3.5 and 4.0 mM were prepared in PBS solution at pH 7.0. The concentrations of H₂O₂ were stored at low temperatures < 10 °C in a refrigerator. The determination of H₂O₂ was performed by cyclic voltammetry at a potential range from -0.6 to 0.6 V at 50 mV/s for one cycle.

Chapter 3

Results & Discussion

3.1 Structural and morphological characterization

3.1.1 Fourier transform infrared (FTIR) spectroscopy

Figures 3.1 and 3.2 show the FTIR spectra of pristine carbon nanotubes (CNTs) (3.1a), functionalized CNTs (3.1b), and zirconia doped carbon nanotubes (ZrO_2 -CNTs) nanostructure system (3.1c).

FTIR spectra (3.1) shows similar spectra for each sample, it can be attributed to the weak charge difference between the carbon atoms due to the high symmetry of CNTs which generates weak signals in the infrared spectrum.[45] Furthermore, there are not the presence of bands corresponding to functional groups this is due to the small number of functional groups on the walls of CNTs and ZrO_2 -CNT. In figure 3.2a,b, the fingerprint of CNTs is found in a range of 400 to 600 cm^{-1} , moreover in figure 3.2c the band between 400 - 480 cm^{-1} corresponds to Zr-O-Zr bond and its vibration is found between 645 - 450 cm^{-1} , thus the presence of ZrO_2 on the CNTs is proved. The main difference between ZrO_2 -CNTs and CNTs spectrum is observed in the range of 400 - 950 cm^{-1} , it is probably because of a chemical interaction between ZrO_2 and the walls of CNTs.[45]

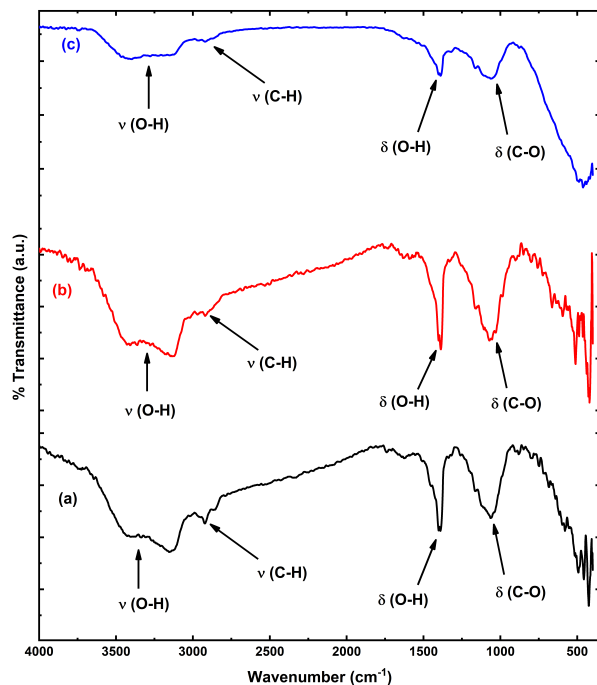


Figure 3.1: FTIR spectra of (a) pristine CNTs, (b) functionalized CNTs and (c) ZrO_2 -CNTs in a range from 4000 to 400 cm^{-1}

Moreover, the bands at 3300 cm^{-1} , 2922 cm^{-1} , 1390 cm^{-1} , and 1060 cm^{-1} correspond to O–H stretching ($\nu(\text{O-H})$), C–H stretching ($\nu(\text{C-H})$), O–H bending ($\delta(\text{O-H})$) and C–O bending ($\delta(\text{C-O})$), respectively.[45] Those bands belong to the alcohol compounds, isopropanol and zirconium isopropoxide, and acids used during the synthesis and functionalization process. FTIR spectra of pristine CNTs show high intense peaks compared to the ZrO_2 -CNTs, this is because of the thermal treatment process carried out during the synthesis of ZrO_2 -CNTs.

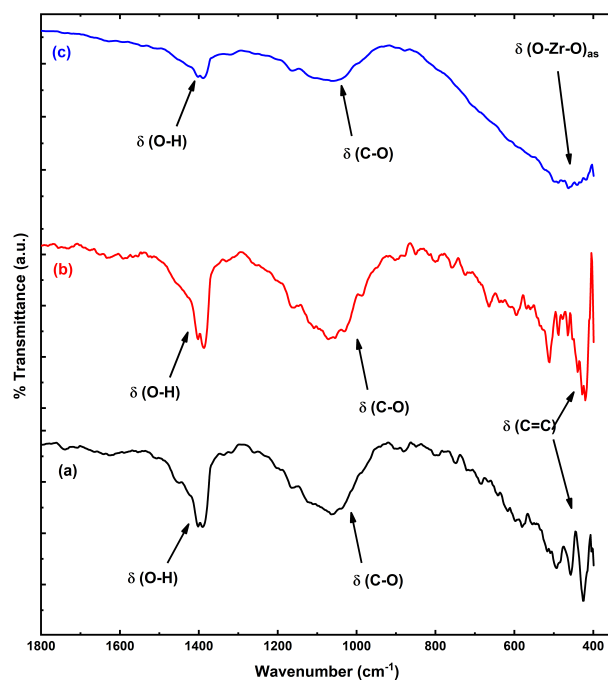


Figure 3.2: FTIR spectra of (a) pristine CNTs, (b) functionalized CNTs and (c) ZrO_2 -CNTs in a range from 1800 - 400 cm^{-1}

3.1.2 X-ray diffraction (XRD) spectroscopy

Figure 3.3 shows the diffraction pattern of pristine CNTs, functionalized CNTs and zirconia doped carbon nanotubes (ZrO_2 -CNTs) nanostructure system. The main features of XRD pattern of CNTs (Figure 3.3 a-b) are similar to those of graphite due to their intrinsic nature, therefore the peaks at about 25° and 43° corresponds to (002) and (100) of the honeycomb lattice of single graphene sheet. [46] XRD patterns of CNTs do not show other reflections which means the lower presence of carbonaceous impurities or other kind of particle (i.e. metal oxides). The diffraction angle of (002) plane decreases while the interplanar distance and intensity increases as it is shown in table 3.1. It is related to the decrease of outer diameter, presence of the impurity or the alignment of CNTs. [47] In this case, it is because of the degradation of nanotube's wall. The decrease of outer diameter occurs during the functionalization processes owing to the use of acids which also removes the impurities on CNTs. It is also supported by data obtained from TEM images (Table 3.3), where the degradation of nanotube's wall is observable. There is not much difference

between the XRD patterns of pristine (Figure 3.3a) and functionalized (Figure 3.3b) CNTs which indicate that the functionalization processes do not change CNTs structurally.

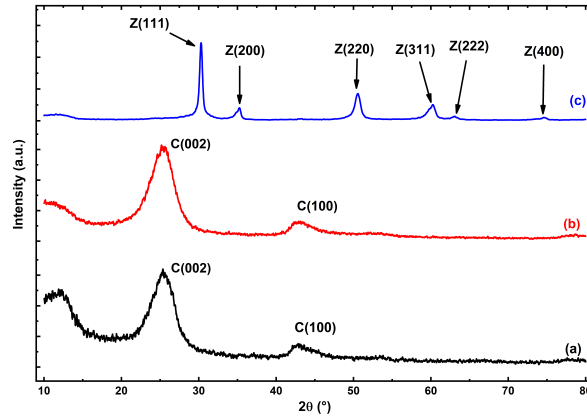


Figure 3.3: XRD pattern of (a) pristine CNTs, (b) functionalized CNTs and (c) ZrO₂-CNTs

Table 3.1: XRD parameters of CNT samples

CNT sample	2θ (°)	d (Å)	FWHM (°)	Intensity (a.u)
Pristine	25.36	3.59	3.96	384
Functionalized	25.18	3.61	3.73	885

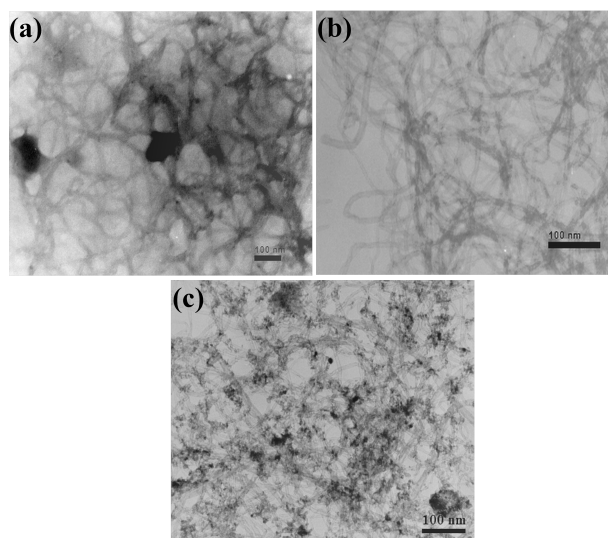
On the other hand, the XRD pattern of ZrO₂-CNTs (Figure 3.3c) shows sharp reflections which means large particle size because of a large aging time. The 2θ values of ZrO₂-CNTs pattern match very well with the values of the cubic phase of ZrO₂ reported Luo *et al.* [48] (Table 3.2). There is no presence of reflections of nanotubes due to the amount of CNTs (36%) respect to ZrO₂ used.

Table 3.2: Diffraction angle values of ZrO-CNTs and ZrO₂, and their miller indexes

Reflection angle (2θ) (°)		Miller index (JCPDS 84-1285)
ZrO ₂ -CNTs	ZrO ₂ cubic phase (JCPDS 27-0997)	
30.30	30.51	(111)
35.25	35.19	(200)
50.54	50.68	(220)
60.24	60.33	(311)
63.08	63.21	(222)
74.62	74.74	(400)

3.1.3 Transmission electron microscopy (TEM)

Transmission electron microscopy (TEM) images of pristine CNTs, functionalized CNTs, and zirconia doped carbon nanotubes (ZrO₂-CNTs) nanostructure system are shown in Figure 3.4.

**Figure 3.4:** TEM images of (a) pristine CNTs, (b) functionalized CNTs, and (c) zirconia doped carbon nanotubes (ZrO₂-CNTs) nanostructure system.

TEM images of CNTs (Figure 3.4 a-b) show that there are no relevant changes in their tubular structures, which means during the prefunctionalization and functionalization processes, the intrinsic structural properties of CNTs

are preserved. According to the characterization made by Sarmiento [42], the diameter of carbon nanotubes (Table 3.3) were decreased from 18 ± 4 to 12 ± 2 nm[42], it means few degradations of nanotube's walls, probably due to the use of acid during the functionalization process.

Figure 3.4c illustrates the ZrO_2 -CNTs nanostructure system in different areas of the sample. The image shows a random distribution of zirconia particles on the wall of CNTs which means a poor distribution of functional groups, as well the agglomeration of nanotubes. The particle size of zirconia measured by Sarmiento [42] was 6.6 ± 1.8 nm.

Table 3.3: Diameter distribution of CNT samples [42]

CNT sample	Diameter (nm)	Distribution of diameter (nm)
Pristine	18 ± 4	12-25
Functionalized	12 ± 2	7-16

3.1.4 Surface area BET

The surface area of functionalized CNTs and zirconia doped carbon nanotubes (ZrO_2 -CNTs) were analyzed. The surface area of CNTs depend on the number of compounds or particles attached to its surface. Large number of particles on the surface means a lower surface area value. The values of surface area obtained were 298 ± 3 m²/g and 92 ± 1 m²/g for the functionalized CNTs and ZrO_2 -CNTs , respectively.

3.2 Electrochemical characterization of CNT based electrodes

3.2.1 Electron transfer behavior of glassy carbon (GC) electrode

To obtain information about the electrochemical processes that occur at the electrode surface, cyclic voltammetry (CV) studies are performed. The $Fe(CN)_6^{4-/3-}$ couple was used for the study due to its fast electron transfer kinetics on many materials including carbon-based electrodes.[9] The effect of scan rate on the electrochemical behavior of the $Fe(CN)_6^{4-/3-}$ redox couple is illustrated in figure 3.5a. CV of the GC electrode exhibits an increase of the redox peak current and the peak-to-peak separation (ΔE_p) increase simultaneously (Table 3.4).

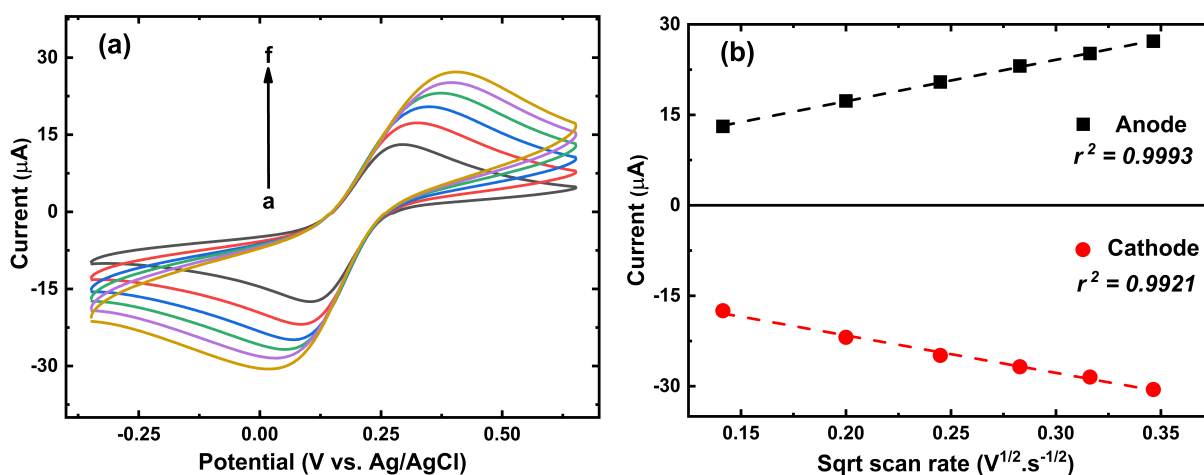


Figure 3.5: (a) Influence of scan rate on the cyclic voltammetric responses of bare GC electrode in 0.1 M PBS (pH 7.0) solution containing 4.0 mM of $K_3[Fe(CN)_6]$ with the scan rates of 20, 40, 60, 80, 100 and 120 mV/s (a-f). (b) Linear relationship of the redox peak currents against root squared scan rate ($v^{1/2}$)

Both anodic and cathodic peak currents increase linearly with respect to scan rate from 20 to 120 mV/s, which implies a diffusion-controlled system.[9] Figure 3.5b shows the linear relationship of the redox peak current with root square scan rate ($v^{1/2}$), this relationship is described by Randles-Sevcik equation (eq. 1.7). Two linear regression equations (eq. 3.1, 3.2) are obtained from the i_p against $v^{1/2}$.

$$i_{pa} = 6.8782 \times 10^{-5} v^{1/2} + 3.4910 \times 10^{-6} \quad (n = 6; r^2 = 0.9993) \quad (3.1)$$

$$i_{pc} = -6.2110 \times 10^{-5} v^{1/2} + 9.1510 \times 10^{-6} \quad (n = 6; r^2 = 0.9922) \quad (3.2)$$

The average geometric area of the electrode can be estimated using the equations 3.1 and 3.2, according to this method, the geometric area value was obtained as 0.024 cm². The effective surface area will increase by addition of layers on the surface of electrode.

On the other hand, the peak-to-peak separation potential (ΔE_p) shifts by increasing the scan rate, then it suggests a quasi-reversible electrode process. [9] Furthermore, the i_{pa}/i_{pc} values are less than one which are typical values of a quasi-reversible behavior of the electrode.[49]

Table 3.4: Data for the effect of scan rate on peak currents and peak potentials of GC electrode

ν (mV/s)	i_{pa} (μ A)	E_{pa} (mV)	i_{pc} (μ A)	E_{pc} (mV)	i_{pa}/i_{pc}	$E^{o'}$ (mV)	ΔE_p (mV)
20	13.09	299	-17.48	107	0.749	203	192
40	17.30	320	-21.89	88	0.790	204	232
60	20.45	348	-24.89	69	0.822	209	279
80	23.10	371	-26.77	58	0.863	215	313
100	25.16	392	-28.47	36	0.884	214	356
120	27.21	402	-30.55	29	0.891	216	373

3.2.2 Capacitance evaluation of glassy carbon (GC) electrode

Figure 3.6 shows the cyclic voltammetry of the bare GC electrode in the region without faradaic current and its linear regression in a potential range from -0.14 to 0.5 V. Figure 3.5a illustrates the increasing of background current (charging current) respect to the scan rate, it means the background current is function of scan rate, and it is described by the equation 2.1.

The plot of current density (i_c/A) against scan rate (ν) (Figure 3.6b) gave a straight line with a slope of 0.41 mF/cm², which is the double-layer capacitance (C_{dl}) of the electrode. According to the equation 2.1, the capacitance of the electrode will depend on the geometric area of the electrode, therefore in the following sections, the addition of layers on the GC electrode will increase the double layer capacitance.[50]

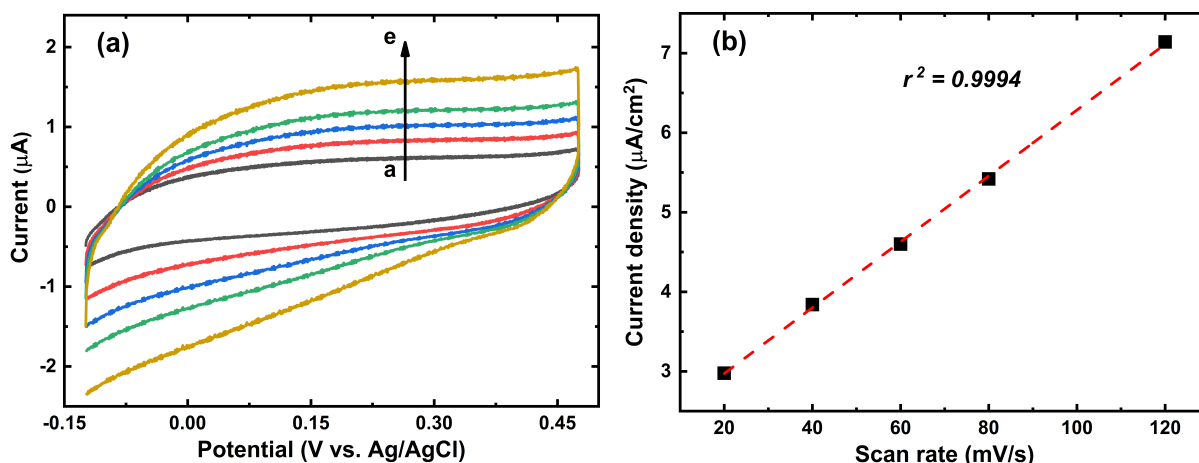


Figure 3.6: (a) Scan rate influence on the background current of bare GC electrode in 0.1 M PBS (pH 7.0) solution with the scan rates of 20, 40, 60, 80 and 120 mV/s (a-e). (b) Linear relationship of the anodic currents against scan rate (ν)

3.2.3 Electron transfer behavior of PDDA/CNTs/GC electrode

Figure 3.7 shows the progressive increase of redox current peaks (i_p) respect to scan rate (ν). The linear relationship of the scan rate and cathodic and anodic current peaks are show in figure 3.7b.

The inspection of cyclic voltammetry data (Table 3.5) suggests a quasi-reversible electrode process, however as expected, the peak-to-peak separation potential is decreased compared to the bare GC electrode, which means that the electron transfer is improved by the addition of CNTs. Two linear regression equations (eq. 3.3, 3.4) are obtained from the i_p against $\nu^{1/2}$ plots.

$$i_{pa} = 1.84 \times 10^{-3} \nu^{1/2} - 1.4156 \times 10^{-4} \quad (n = 6; r^2 = 0.9954) \quad (3.3)$$

$$i_{pc} = -2.20 \times 10^{-3} \nu^{1/2} + 1.6061 \times 10^{-4} \quad (n = 6; r^2 = 0.9961) \quad (3.4)$$

The average geometric area of the electrode is estimated using the linear regressions, according to this method, the geometric area value was obtained as 0.65 cm².

The main observation in the cyclic voltammograms of the CNTs modified electrode is the increase of the anodic and cathodic current values, it is because of the addition of layers of nanotubes and PDDA onto the surface of

the electrode; moreover, CNTs provide large surface area due to its tubular structure and excellent electron-transfer properties.

The nanotubes layer induces high non-faradic current values, however the high non-faradic current could overlap reactions that occur at low current scales. In order to decrease the non-faradic current, the surface area of CNTs should be decreased by functionalization[51] or modification with nanoparticles (NPs) as it is done in this work.

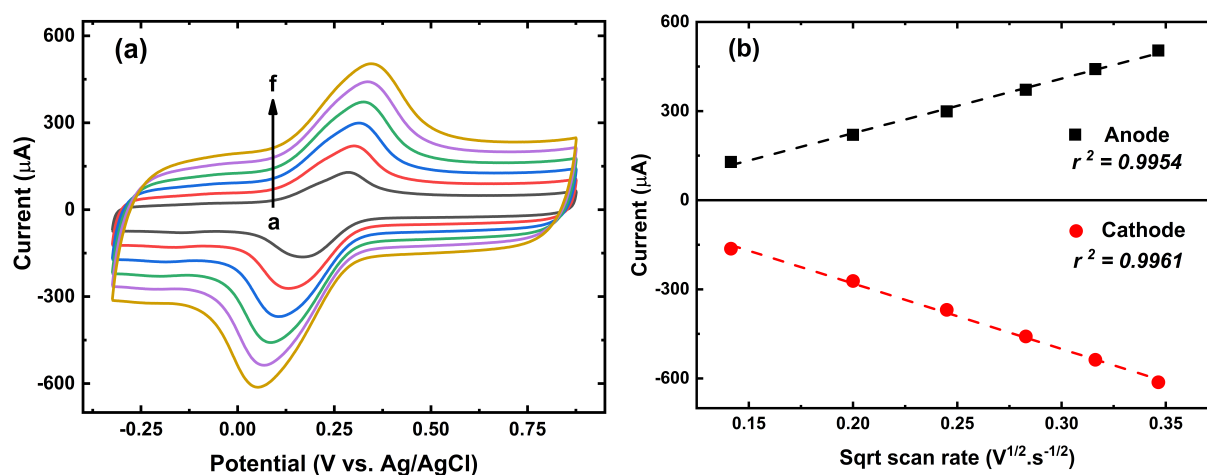


Figure 3.7: (a) Cyclic voltammograms of PDDA/CNTs/GC electrode in 0.1 M PBS (pH 7.0) solution containing 4.0 mM of $K_3[Fe(CN)_6]$ with the scan rates of 20, 40, 60, 80, 100 and 120 mV/s (a-f). (b) Linear relationship of the redox peak currents against root squared scan rate ($v^{1/2}$)

Table 3.5: Data for the effect of scan rate on peak currents and peak potentials of PDDA/CNTs/GC electrode

v (mV/s)	i_{pa} (μA)	E_{pa} (mV)	i_{pc} (μA)	E_{pc} (mV)	i_{pa}/i_{pc}	E° (mV)	ΔE_p (mV)
20	129	286	-163	170	0.788	228	116
40	220	300	-272	134	0.809	217	166
60	299	314	-369	106	0.810	210	208
80	372	326	-459	87	0.811	207	239
100	441	335	-537	68	0.822	202	267
120	504	344	-613	54	0.822	199	290

3.2.4 Capacitance evaluation of PDDA/CNTs/GC electrode

Cyclic voltammograms of the non-faradic current of the PDDA/CNTs/GC electrode is shown in the figure 3.8. The non-faradic current of the electrode increases as mentioned in the previous section (3.2.3). Furthermore, the double layer capacitance increases compared to the bare glassy carbon electrode as expected. The linear regression (Figure 3.8b) allowed to calculate the double layer capacitance which is 2.37 mF/cm^2 for the PDDA/CNTs/GC electrode. The double layer capacitance depend on the geometric area of the electrode which is large for this electrode (0.65 cm^2).

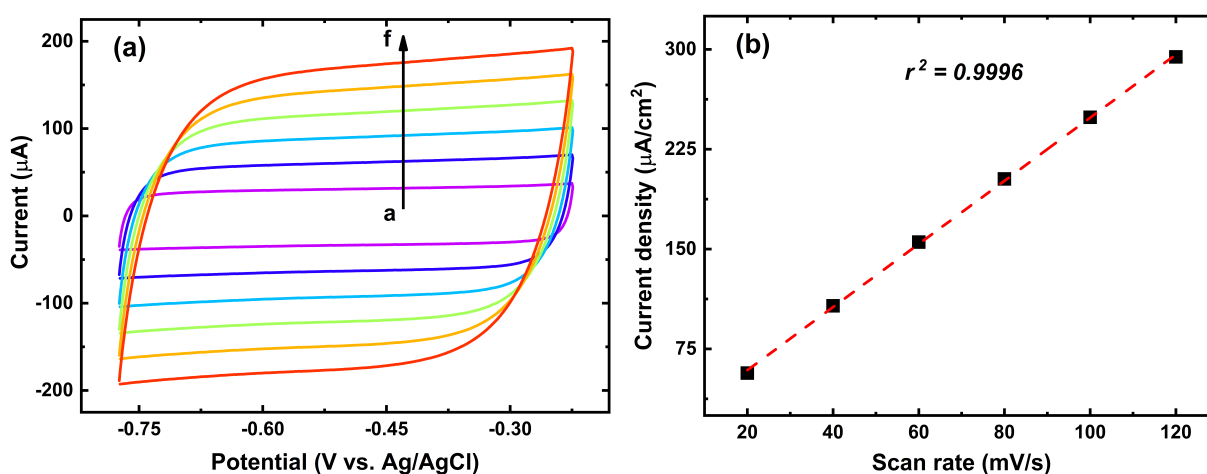
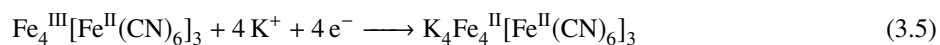


Figure 3.8: (a) Scan rate influence on the background current of PDDA/CNTs/GC electrode in 0.1 M PBS (pH 7.0) solution with the scan rates of 20, 40, 60, 80, 100 and 120 mV/s (a-f). (b) Linear regression of the anodic currents against scan rate (ν)

3.2.5 Electron transfer behavior of PDDA/PB/PDDA/CNT/GC electrode

The electron transfer behavior of Prussian blue (PB) electrodeposited on the CNTs modified electrode is shown in figure 3.9. A pair of well-defined redox peaks were observed with the potentials at $E_{pa} = 0.27 \text{ V}$ and $E_{pc} = 0.13 \text{ V}$ at a scan rate of 40 mV/s (Table 3.6). The CVs for the redox reaction of PB on the CNTs modified electrode at various scan rates is shown in the figure 3.9a. The peaks observed in the voltammograms (Figure 3.9a) belong to the reduction and oxidation states of Prussian blue. Prussian blue ($\text{Fe}_4^{\text{III}}[\text{Fe}^{\text{II}}(\text{CN})_6]_3$) in its reduced form is known

as Prussian white ($\text{Fe}^{\text{II}}[\text{Fe}^{\text{II}}(\text{CN})_6]_3^{4-}$). The redox reaction can be expressed as follows:



Initially PB is not a charged structure but the reduced form, Prussian white, has a negative charge which is compensated by a cation as is shown in the redox reaction.

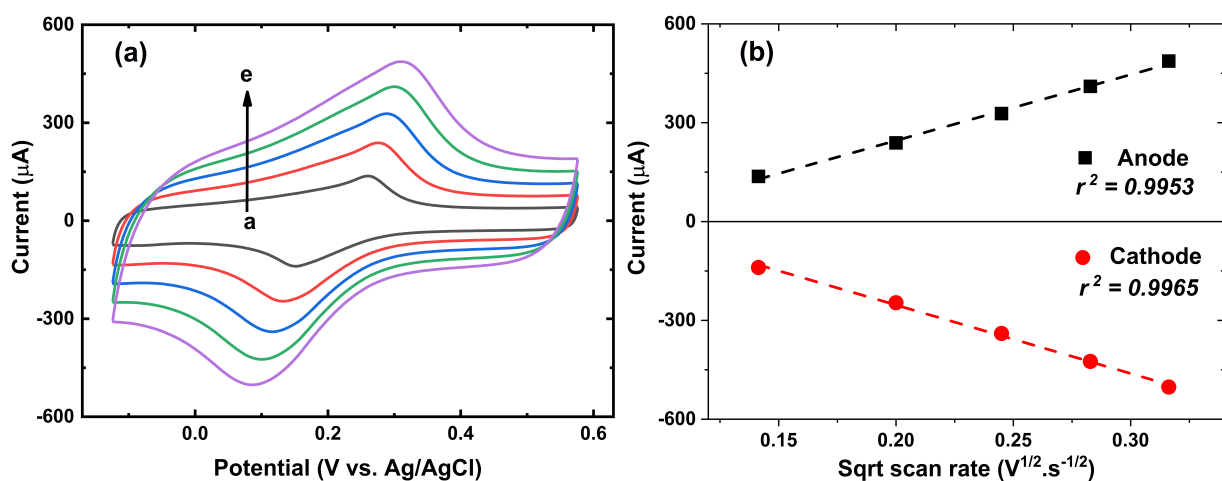


Figure 3.9: (a) Cyclic voltammograms of PDDA/PB/PDDA/CNTs/GC electrode in 0.1 M PBS (pH 7.0) solution with the scan rates of 20, 40, 60, 80 and 100 mV/s (a-e). (b) Linear relationship of the redox peak currents against root squared scan rate ($\nu^{1/2}$).

It can be observed that the peak currents increased with the increase of scan rates, simultaneously, the cathodic and anodic peak potentials exhibit small shift and the peak current increases along with the rising of scan rate from 10 to 100 mV/s. As shown in the figure 3.9b, the cathodic and anodic peak currents increase linearly with the scan rate. All these facts demonstrate that the reactions on PDDA/PB/PDDA/CNTs/GC electrode are diffusion-controlled and quasi-reversible process between the PB and PDDA/CNTs films.

Table 3.6: Data of the effect of scan rate on peak currents and peak potentials PDDA/PB/PDDA/CNTs/GC electrode

ν (mV/s)	i_{pa} (μ A)	E_{pa} (mV)	i_{pc} (μ A)	E_{pc} (mV)	i_{pa}/i_{pc}	E° (mV)	ΔE_p (mV)
20	137	260	-139	153	0.983	331	107
40	239	276	-247	134	0.968	329	142
60	328	288	-340	116	0.964	326	172
80	410	300	-425	101	0.966	325	199
100	487	309	-502	87	0.969	322	222

3.2.5.1 Electron transfer behavior comparison of modified electrodes

The electron transfer behavior of modified electrodes was monitored by cyclic voltammetry experiments (Figure 3.10). The background current increases after the addition of CNTs to the GC electrode, it is because of the high surface area and excellent electron-transfer properties of CNTs. Afterwards, the electrodeposition of PB on the PDDA/CNTs/GC electrode induces electrochemical changes on the electrodes, for instance, the redox peaks of PDDA/PB/PDDA/CNTs/GC electrode are sharper and potentials are shifted compared to bare GC and PDDA/CNTs/GC electrode.

The addition of electroactive layers onto the surface of the GC electrode enhanced the current response and electron transfer. For instance, the peak-to-peak separation potential values at 40 mV/s are 232 mV, 166 mV and 142 mV (see Table 3.4, 3.5 and 3.6) for bare GC, PDDA/CNTs/GC, and PDDA/PB/PDDA/CNTs/GC electrodes, respectively, it means that the reversibility of the electrode is gradually improved due to the addition of electroactive compounds (CNTs and PB).

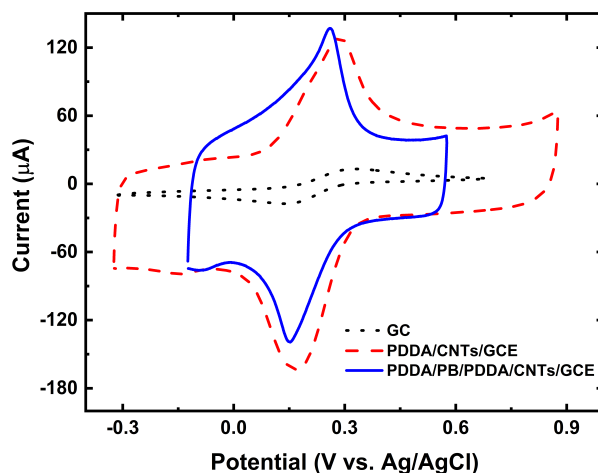


Figure 3.10: Cyclic voltametry of bare GC electrode (dotted line), PDDA/CNTs/GC electrode (dashed line), and PDDA/PB/PDDA/CNTs/GC electrode (solid line) in 0.1 M PBS (pH 7.0) containing 4.0 mM of $K_3[Fe(CN)_6]$ at 40 mV/s.

3.3 Electrochemical characterization of Zirconia-CNT based electrodes

3.3.1 Electron transfer behavior of PDDA/ ZrO_2 -CNTs/GC electrode

Cyclic voltammograms of PDDA/ ZrO_2 -CNTs/GC electrode in 0.1 M PBS (pH 7.0) solution containing 4.0 mM $K_3[Fe(CN)_6]$ with different scan rates (10 - 120 mV/s) were investigated, and the curves are shown in figure 3.11. The cathodic and anodic peak currents increase, at the same time, the scan rate increases (Figure 3.11a). The redox peak potentials show a small shift, with peak-to-peak separation potential becoming enlarged (Table 3.7). The results indicate that the PDDA/ ZrO_2 -CNTs/GC electrode promotes a quasi-reversible and diffusion-controlled processes. Figure 3.11b shows that the redox peak currents increased linearly with the scan rate. Two linear regression equations (eq. 3.6, 3.7) are obtained from the i_p vs. $\nu^{1/2}$ plots.

$$i_{pa} = 4.9579 \times 10^{-4} \nu^{1/2} - 2.4174 \times 10^{-5} \quad (n = 6; r^2 = 0.9978) \quad (3.6)$$

$$i_{pc} = -5.3518 \times 10^{-4} \nu^{1/2} + 1.7293 \times 10^{-5} \quad (n = 6; r^2 = 0.9981) \quad (3.7)$$

The average of geometric area can be calculated from these linear regressions, using this method, the geometric area (A) value was obtained as 0.17 cm^2 . The area of this electrode is lower than the PDDA/CNTs/GC electrode.

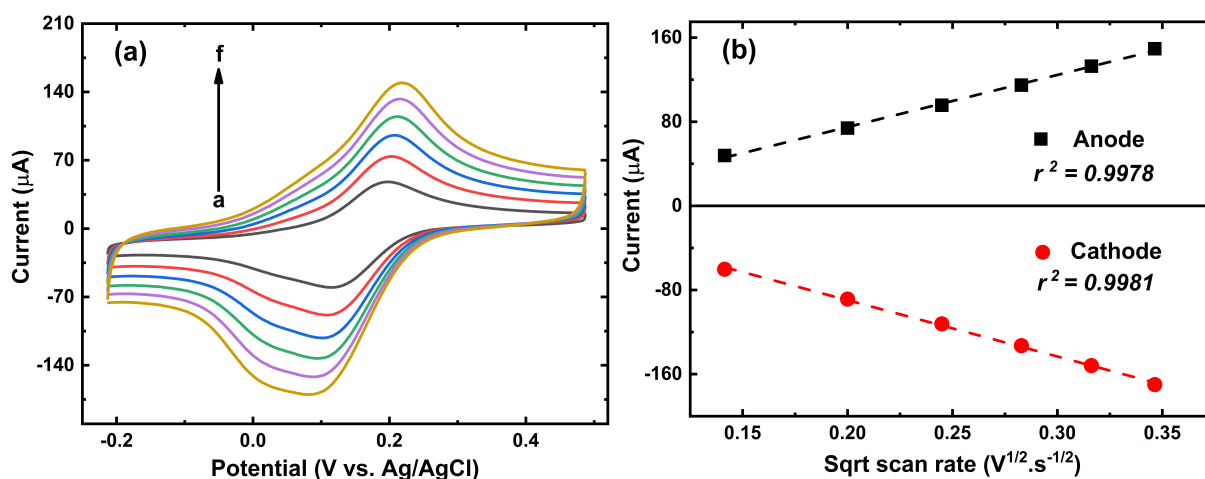


Figure 3.11: (a) Cyclic voltammograms of PDDA/ZrO₂-CNTs/GC electrode in 0.1 M PBS (pH 7.0) solution containing 4.0 mM of K₃[Fe(CN)₆] with the scan rates of 20, 40, 60, 80, 100 and 120 mV/s (a-f). (b) Linear relationship of the redox peak currents versus root squared scan rate ($\nu^{1/2}$).

Table 3.7: Data for the effect of scan rate on peak currents and peak potentials of the PDDA/ZrO₂-CNTs/GC electrode

ν (mV/s)	i_{pa} μA	E_{pa} (mV)	i_{pc} μA	E_{pc} (mV)	i_{pa}/i_{pc}	E° (mV)	ΔE_p (mV)
20	47.87	196	-60.30	116	0.794	156	80
40	73.91	201	-88.66	106	0.834	154	95
60	95.65	208	-112.2	102	0.852	155	106
80	114.80	213	-133.0	97	0.863	155	116
100	132.80	215	-151.9	92	0.874	154	123
120	149.40	218	-170.0	85	0.878	150	130

3.3.2 Capacitance evaluation of PDDA/ZrO₂-CNTs/GC electrode

Figure 3.12 shows the influence of the scan rate on the non-faradic of PDDA/ZrO₂-CNTs/GC electrode. The linear regression provides the value of double layer capacitance which is 1.51 mF/cm².

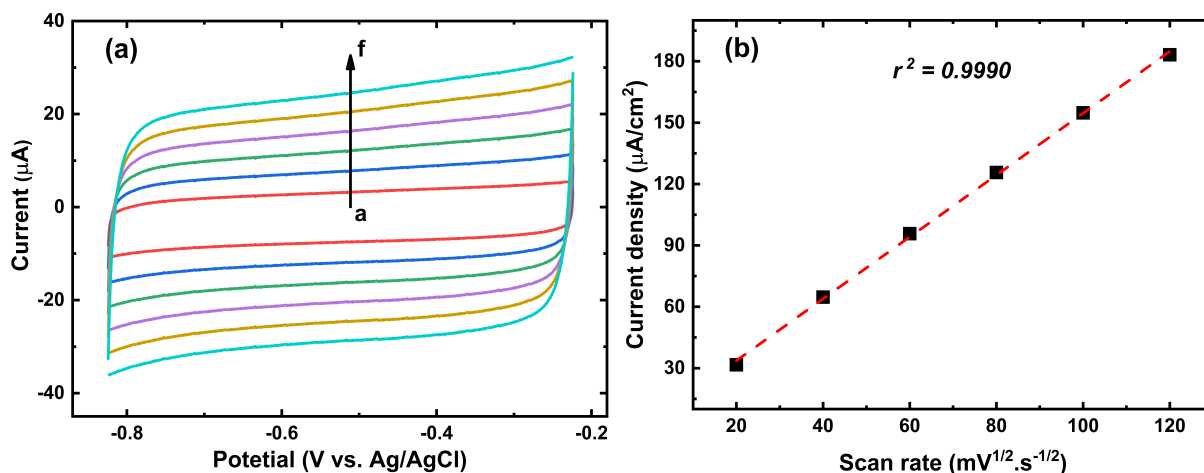


Figure 3.12: (a) Scan rate influence on the background current of PDDA/ZrO₂-CNTs/GC electrode in 0.1 M PBS (pH 7.0) solution with the scan rates of 20, 40, 60, 80 and 120 mV/s (a-f). (b) Linear regression of the anodic currents versus scan rate (ν).

The double layer capacitance and geometric area values for the PDDA/ZrO₂-CNTs/GC electrode are 1.51 mF/cm² and 0.17 cm², respectively. These values are small compared to the PDDA/CNTs/GC electrode, this result is attributed to the lower surface area of the ZrO₂-CNTs, and it is probably related to the number of particles attached to the nanotube's wall. From the surface area BET analysis, the ZrO₂-CNTs surface area, 92 ± 1 m²/g, is lower than the CNTs surface area, 298 ± 3 m²/g. therefore the non-faradic current decreases due to the smaller surface area of ZrO₂-CNTs. Although, the decrease of the non-faradic current has its advantages, for instance low double layer capacitance means high detection limit of the sensor,[50] and the reactions that might occur at micro ampere scale will be able to be determined, and quantified.

3.3.3 Electron transfer behavior of PDDA/PB/PDDA/ZrO₂-CNTs/GC electrode

The electron transfer behavior of PB electrodeposited on the ZrO₂-CNTs modified electrode is shown in figure 3.13. Redox peaks are found at potentials of $E_{pa} = 0.20$ V and $E_{pc} = 0.11$ V at a scan rate of 40 mV/s (Table 3.8). The CVs for the redox reaction of PB on the ZrO₂-CNTs modified electrode at various scan rates is shown in the figure 3.13a.

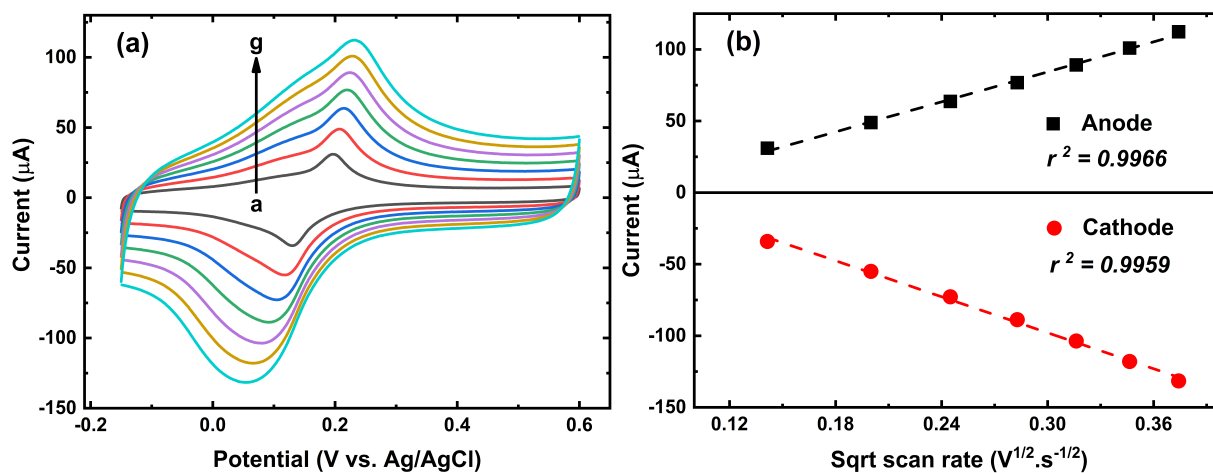


Figure 3.13: (a) Cyclic voltammograms of PDDA/PB/PDDA/ZrO₂-CNTs/GC electrode in 0.1 M PBS (pH 7.0) solution containing 4.0 mM of K₃[Fe(CN)₆] with the scan rates of 20, 40, 60, 80, 100, 120 and 140 mV/s (a-g). (b) Linear relationship of the redox peak currents versus root squared scan rate ($v^{1/2}$).

As in other cases, the peak currents increased with the increase of scan rates, at the same time, the cathodic and anodic peak potentials are shifted and the peak current increases along with the rising of scan rate from 10 to 140 mV/s (Table 3.8). The linear increase of cathodic and anodic peak currents with the scan rate is shown in figure 3.13b. All these results suggest that the reactions on the PDDA/PB/PDDA/ZrO₂-CNTs/GC electrode are diffusion-controlled and quasi-reversible process.

The redox reaction of PB onto the surface of PDDA/PB/PDDA/ZrO₂-CNTs/GC electrode follow the same reaction expressed in reaction equation 3.5.

Table 3.8: Data for the effect of scan rate on peak currents and peak potentials of PDDA/PB/PDDA/ZrO₂-CNTs/GC electrode

ν (mV/s)	i_{pa} (μ A)	E_{pa} (mV)	i_{pc} (μ A)	E_{pc} (mV)	i_{pa}/i_{pc}	E° (mV)	ΔE_p (mV)
20	31	196	-34	130	0.906	163	66
40	49	206	-55	117	0.887	162	89
60	64	214	-73	104	0.875	159	110
80	77	219	-89	91	0.865	155	128
100	89	224	-104	81	0.859	153	143
120	101	229	-118	66	0.855	148	163
140	112	232	-132	57	0.853	145	175

3.3.3.1 Electron transfer behavior of modified electrodes

Figure 3.14 shows the cyclic voltammograms of the ZrO₂-CNTs based electrodes in 0.1 M PBS (pH 7.0) containing 4.0 mM of K₃[Fe(CN)₆] at 40 mV/s. The increase of the non-faradic currents with a large area demonstrated that the presence of ZrO₂-CNTs layer induces electrochemical changes on the surface of GC electrode. By simple observation, the non-faradic current and redox peak currents are lower than observed in CNTs based electrodes. After addition of PB, the voltammogram (Figure 3.14 - solid line) shows sharp peaks compared to the bare GC and PDDA/ZrO₂-CNTs/GC electrodes, also the background current is decreased, probably because of modifications induced by PB electroactive layer over the ZrO₂-CNTs layer.[3]

However, the peak-to-peak separation potentials at 40 mV/s corresponding to the bare GC (232 mV), PDDA/ZrO₂-CNTs/GC (95 mV), and PDDA/PB/PDDA/ZrO₂-CNTs/GC (89 mV) electrodes are improved due to the usage of doped nanotubes and an electroactive surface, PB layer. Those changes make the reaction processes on the electrode more reversible, moreover it is supported by the ratio of the redox peak current at 40 mV/s of the bare GC ($i_{pa}/i_{pc} = 0.79$), PDDA/ZrO₂-CNTs/GC ($i_{pa}/i_{pc} = 0.83$), and PDDA/PB/PDDA/ZrO₂-CNTs/GC ($i_{pa}/i_{pc} = 0.88$) electrodes.

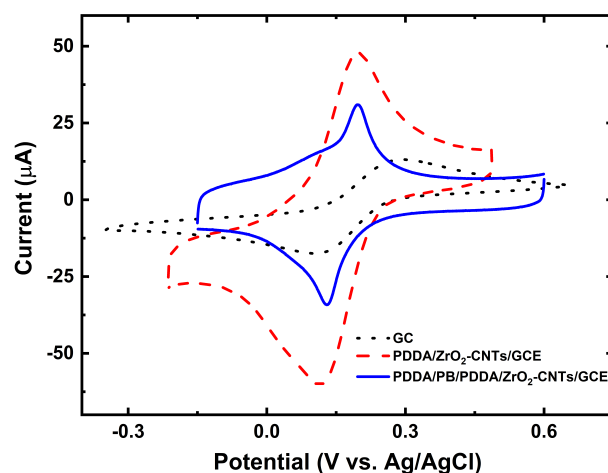


Figure 3.14: Cyclic voltammetry of bare GC electrode (dotted line), PDDA/ZrO₂-CNTs/GC electrode (dashed line), and PDDA/PB/PDDA/ZrO₂-CNTs/GC electrode (solid line) in 0.1 M PBS (pH 7.0) containing 4.0 mM of K₃[Fe(CN)₆] at 40 mV/s.

3.4 Electrochemical detection of hydrogen peroxide on the modified electrodes

3.4.1 Hydrogen peroxide detection in PDDA/CNTs/GC electrode

Figure 3.15 shows the cyclic voltammograms of the PDDA/CNTs/GC electrode in 0.1 M PBS (pH 7.0) containing H₂O₂ at different concentrations. The reduction peak current should be observed at about -0.28 V vs. Ag/AgCl.[7] In the voltammogram there is not an increase of the reduction peak due to the lack of electron mediator, however, there are researches which report H₂O₂ detection using CNTs modified electrode.[52] Mainly, the nanotube surface needs to be activated by several cycles and in an acid media in order to be used as H₂O₂ catalyst.

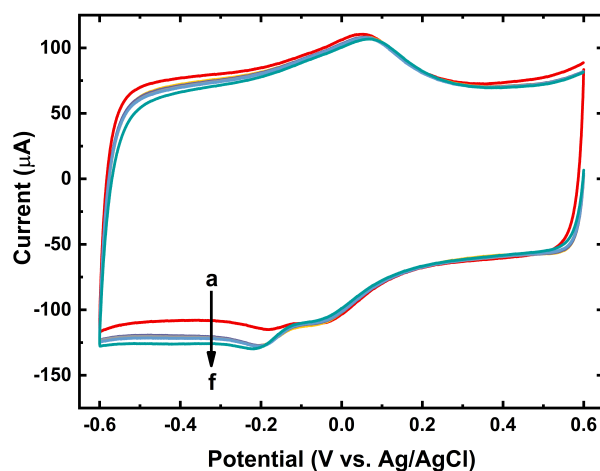


Figure 3.15: Cyclic voltammograms of PDDA/CNTs/GC electrode in the presence of different concentrations of H_2O_2 (0.0, 0.5, 1.0, 1.5, 2.0 and 2.5 mM) (a-f) with the scan rate at 50 mV/s

Moreover, there are a pair of redox peaks at 0.05 V and 0 V, which correspond to the redox reaction of quinone functional group, which are impurities attached to the surface of carbonaceous materials.[51] The quinone functional groups are easily adsorbed to a carbon based material.[53]

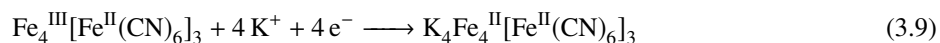
3.4.2 Hydrogen peroxide detection in PDDA/PB/PDDA/CNTs/GC electrode

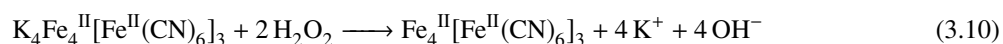
3.4.2.1 Cyclic voltammetry detection and electrocatalytic activity of PB

As it was mentioned, PB can be used to reduce/oxidize H_2O_2 through electrochemical catalyst. PB is considered as an artificial peroxidase. Figure 3.16a shows a reduction peak at about 0.084 V and oxidation peak at 0.217 V. The reduction peak increases with the addition of H_2O_2 concentration in the range of 1.0 - 3.5 mM, and the linear regression equation is stated below (eq. 3.8).

$$i_{pc} = -5.9142 \times 10^{-3} C - 1.109 \times 10^{-4} \quad (n = 6; r^2 = 0.9961) \quad (3.8)$$

The reduction peak current value increases while the oxidation peak current decreases by addition of hydrogen peroxide which demonstrates a typical electrocatalytic reduction of H_2O_2 . [3] According to the literature [3], [4], [5] the electrocatalytic process is as follows:





Reactions 3.9, 3.10 and 3.11 show, first the reduction of PB towards PW (eq. 3.9), then PW reacts with the H_2O_2 producing OH^- and PB returns to its initial state (eq. 3.10), finally, the reduction of H_2O_2 follows the 2-electron reduction (eq. 3.11).

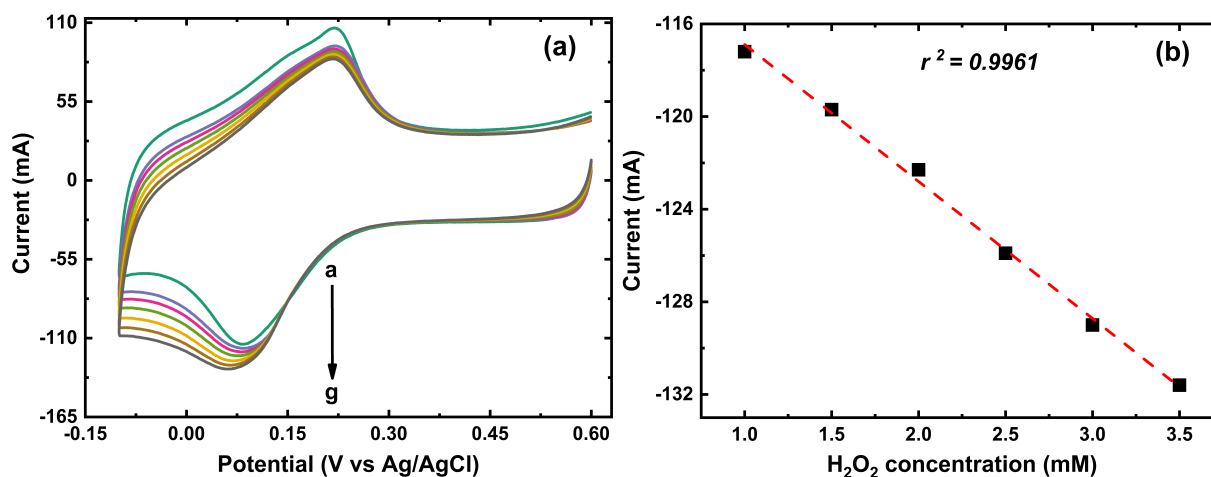


Figure 3.16: (a) Cyclic voltammograms of PDDA/PB/PDDA/CNTs/GC electrode in the presence of different concentrations of H_2O_2 (0.0, 1.0, 1.5, 2.0, 2.5, 3.0 and 3.5 mM) (a-g) with the scan rate at 50 mV/s. (b) Calibration curve for the determination of H_2O_2 .

3.4.2.2 Amperometric studies

Amperometric detection proceeded with the modified electrode in a stirred solution at an applied potential of +0.5 V, and the background current was first allowed to decay to a steady-state value. Figure 3.17a shows a typical amperometric response at +0.5 V of the PDDA/PB/PDDA/CNTs/GC electrode to successive addition of 100 μL of 0.1 M H_2O_2 to stirred 0.1 M PBS (pH 7.0). The modified electrode response favorable and rapidly to the concentration of H_2O_2 . The calibration curve of the H_2O_2 concentration respect to anodic current at +0.5 V is shown in figure 3.17b which reveals an excellent linear relationship between the current and the H_2O_2 concentration. The linear regression equation is following: $i = 0.1650 \times 10^{-3} C + 11.3296 \times 10^{-9}$ ($n = 20$; $r^2 = 0.9999$). The linear range of the calibration curve is from 0.50 mM to 9.09 mM with a limit of detection of 0.778 mM (S/N = 3),

and a sensitivity of 0.17 mA M^{-1} . The excellent linear relationship, low detection limit and rapid response (4 s) can be attributed to the excellent electric contact between the GC electrode and the CNTs, PDDA and PB.

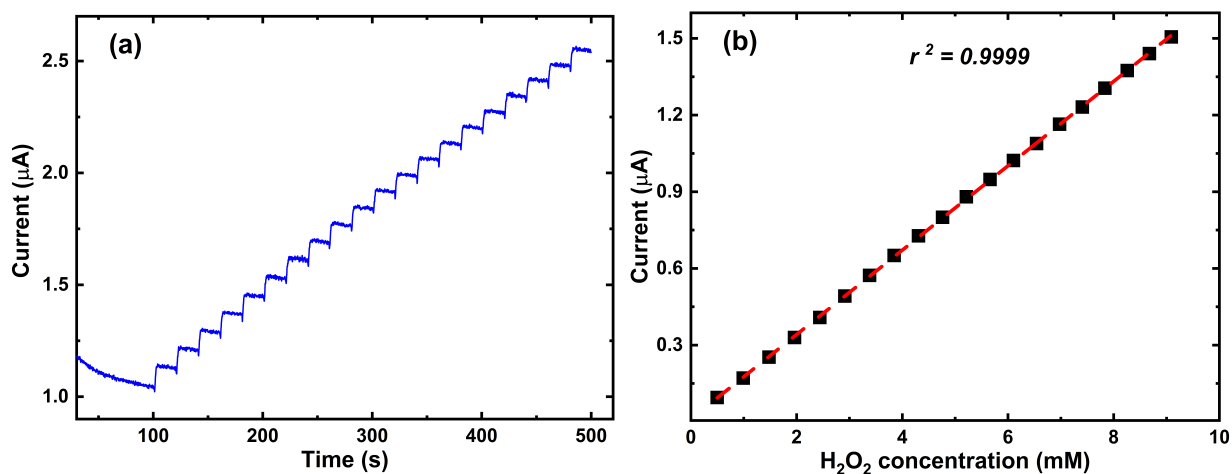


Figure 3.17: (a) Amperometric response of PDDA/PB/PDDA/CNTs/GC electrode in stirred solutions to the successive additions of H₂O₂. (b) Calibration curve

3.4.3 Hydrogen peroxide detection in PDDA/ZrO₂-CNTs/GC electrode

The electrocatalytic reactivity of the PDDA/ZrO₂-CNTs/GC electrode towards H₂O₂ was investigated by CVs at 50 mV/s. As shown in figure 3.18a, when H₂O₂ concentration increases, simultaneously, an increase of the reduction peak at about -0.27 V is observed. The reduction peak current value increases with the increasing concentration of H₂O₂ with a sensitivity of 5.3 mA/M in the linear range of concentration from 1.0 to 4.0 mM. The linear regression equation obtained is stated in the equation 3.12.

$$i_p = -0.0035 C - 4.66 \times 10^{-5} \quad (n = 7; \quad r^2 = 0.9334) \quad (3.12)$$

The response of ZrO₂ surface to reduction of H₂O₂ have been studied previously. [54], [55], [56] Since H₂O₂ can acts as an oxidant or reductant, redox reaction of Zr by reaction of H₂O₂ with ZrO₂ have been proposed. [54] Lousada and Jonsson [54] proposed a metal-oxide-catalyzed reaction which follows the next reaction:



Where M_xO_y is the metal oxide, in this case the zirconium in ZrO_2 is in its highest oxidation state, and only acts as a catalyst.

Finally, the increased peak current of hydrogen peroxide reduction suggest that ZrO_2 doped CNTs nanostructure has catalytic ability for H_2O_2 reduction. Therefore, ZrO_2 are suitable as mediators to shuttle electrons between H_2O_2 and GC electrode, and facilitate electrochemical regeneration following electrons exchange with H_2O_2 .

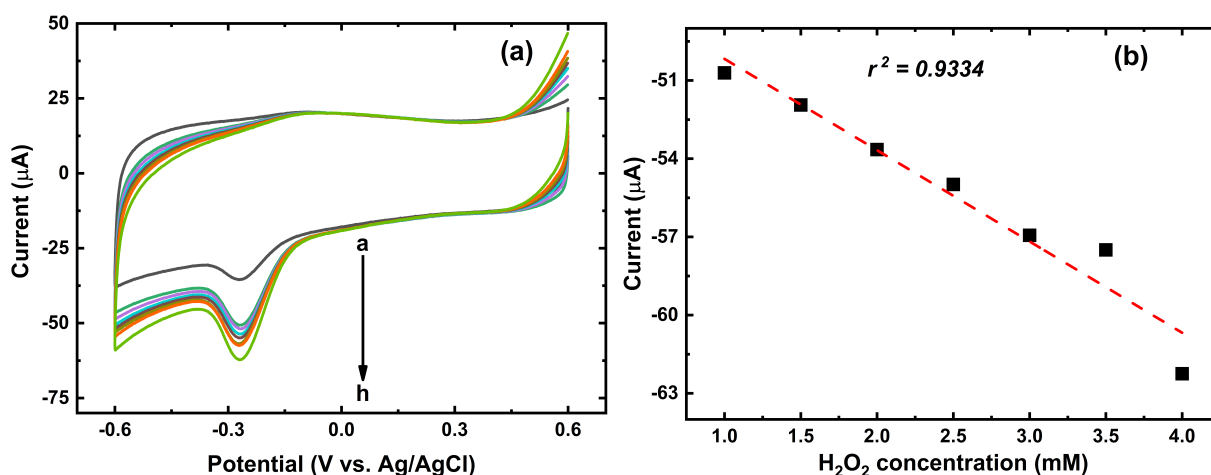


Figure 3.18: (a) Cyclic voltammograms of PDDA/ ZrO_2 -CNTs/GC electrode in the presence of different concentrations of H_2O_2 (0.0, 1.0, 1.5, 2.0, 2.5, 3.0, 3.5 and 4.0 mM) (a-h) with the scan rate at 50 mV/s. (b) Calibration curve for the determination of H_2O_2 .

3.4.4 Hydrogen peroxide detection in PDDA/PB/PDDA/ ZrO_2 -CNTs/GC electrode

3.4.4.1 Cyclic voltammetry detection and electrocatalytic activity of PB

Figure 3.19 shows the cyclic voltammogram (Figure 3.19a) and the calibration curve (Figure 3.19b) of the PDDA/PB/PDDA/ ZrO_2 -CNTs/GC electrode in order to measure the electrocatalytic activity of the electrode. The sequence addition of concentrations of H_2O_2 results in the increase of reduction peak current while the oxidation peak current decreases. The reduction peak observed at about 0.07 V corresponds to the PB reduced form, PW, which follow the reactions equation 3.10, then the oxidation peak appeared at 0.2 V which belong to PB oxidation.

The linear regression equation obtained is as follows (eq. 3.14).

$$i_p = -0.00486 C - 8.8072 \times 10^{-5} \quad (n = 6; r^2 = 0.9970) \quad (3.14)$$

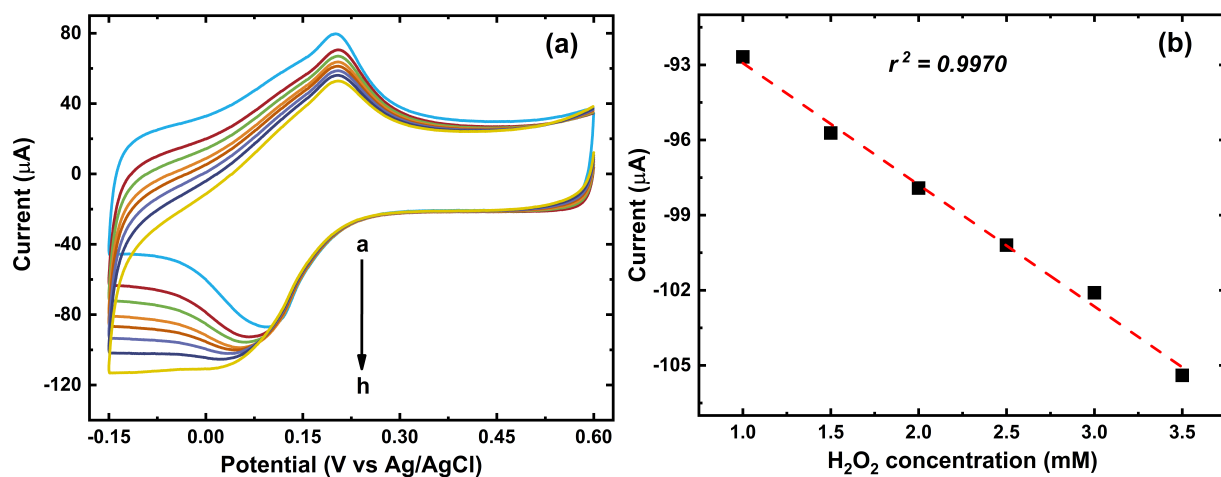


Figure 3.19: (a) Cyclic voltammograms of PDPA/PB/PDPA/ZrO₂-CNTs/GC electrode in the presence of different concentrations of H₂O₂ (0.0, 1.0, 1.5, 2.0, 2.5, 3.0, 3.5 and 4.0 mM) with the scan rate at 50 mV/s. (b) Calibration curve for the determination of H₂O₂.

3.4.4.2 Amperometric studies

Figure 3.20a exhibits the amperometric response of the PDPA/PB/PDPA/ZrO₂-CNTs/GC electrode upon the successive addition of H₂O₂ to 0.1 M PBS (pH 7.0) at an applied potential of +0.5 V.

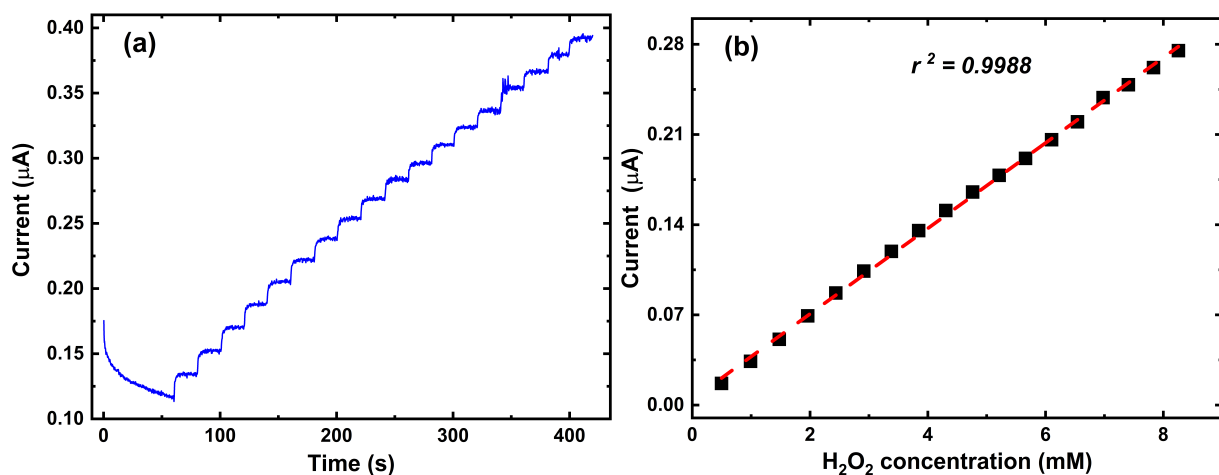


Figure 3.20: (a) Amperometric response of PDDA/PB/PDDA/ZrO₂-CNTs/GC electrode in stirred solutions to the successive additions of H₂O₂. (b) Calibration curve

The electrocatalytic currents of the sensor were observed after each addition of H₂O₂ to the solution. The linear regression equation obtained was: $i = 33.17 \times 10^{-6} C + 4.434 \times 10^{-9}$ ($n = 18$; $r^2 = 0.9988$). The linear range of the sensor based on the calibration curve was between 0.50 - 8.26 mM with a detection limit of 0.135 mM ($S/N = 3$), and a sensitivity of $33.17 \mu\text{A M}^{-1}$. The hydrogen peroxide sensor based on PB deposited on PDDA/ZrO₂-CNTs/GC electrode showed a fast amperometric response (4 s) and high sensitivity. The limit of detection of PDDA/PB/PDDA/ZrO₂-CNTs/GC electrode is higher than the PDDA/PB/PDDA/CNTs/GC electrode, but the sensitivity is lower.

Chapter 4

Conclusions

The ZrO₂-CNT nanostructure system showed zirconia particles with cubic crystalline phase and particle size of 6.6 ± 1.8 nm. During the synthesis of ZrO₂-CNT, the aging time influence in the crystal size. However, the surface area of ZrO₂-CNT is smaller than the surface area of CNTs, and the decrease of surface area is attributed to the large number of zirconia nanoparticles.

It was proved that the carbon nanotubes (CNTs) and zirconia doped carbon nanotube (ZrO₂-CNT) improved the electron transfer behavior of glassy carbon (GC) electrode. CNTs modified electrode shows a large non-faradic current, which means that the surface of GC electrode was modified electrochemically by the CNTs. On the other hand, the ZrO₂-CNT shows small non-faradic current due to the lower value of surface area and geometric area of ZrO₂-CNT.

The reduced surface area of CNTs by *in situ* zirconia nanoparticles synthesis induces changes in the electron transfer behavior. The ZrO₂-CNTs modified electrode shows a low peak-to-peak separation potential and an enhanced reversibility of redox reactions as shown by the results in table 3.8.

Furthermore, the CNTs and ZrO₂-CNTs layers exhibit good compatibility and affinity to the PB layer.

It was demonstrated the applicability of the sensor for detection of hydrogen peroxide on Prussian blue (PB) and CNTs based GC electrodes and PDDA/ZrO₂-CNTs/GC electrode by both cyclic voltammetry and amperometry techniques. The findings demonstrate that PB and ZrO₂-CNTs based electrode shown an enhanced limit of detection, 0.135 mM, compared to the PB and CNTs based electrode, 0.778 mM. However, the PB and CNTs based electrode shown a high sensitivity, 0.17 mA M⁻¹, respect to the ZrO₂-CNTs, 33.17 μA M⁻¹.

Based on these advantages, the fabricated sensors exhibit good electrochemical sensitivity, reversibility, and excellent

linear relationship, nonetheless the detection limit of the electrode can be improved, especially enhancing the conditions of hydrogen peroxide detection.

From these result it can be inferred that the zirconia doped carbon nanotubes and the modification method of electrodes could be used in the development of enzyme based biosensors.

Funding

This research was funded by CEDIA (Corporación Ecuatoriana para el Desarrollo de la Investigación y la Academia) through the project “Biosensores basados en Nanotubos de carbono modificados para detección de enzimas”, Code: CEPRA XII-2018-14, Biosensores

Bibliography

- [1] Yan, Y.; Miao, J.; Yang, Z.; Xiao, F.-X.; Yang, H. B.; Liu, B.; Yang, Y. Carbon nanotube catalysts: recent advances in synthesis, characterization and applications. *Chemical Society Reviews* **2015**, *44*, 3295–3346.
- [2] Srinivasan, B.; Tung, S. Development and applications of portable biosensors. *Journal of laboratory automation* **2015**, *20*, 365–389.
- [3] Chu, Z.; Liu, Y.; Jin, W. Recent progress in Prussian blue films: Methods used to control regular nanostructures for electrochemical biosensing applications. *Biosensors and Bioelectronics* **2017**, *96*, 17–25.
- [4] Farah, A. M.; Shooto, N. D.; Thema, F. T.; Modise, J. S.; Dikio, E. D. Fabrication of Prussian blue/multi-walled carbon nanotubes modified glassy carbon electrode for electrochemical detection of hydrogen peroxide. *Int J Electrochem Sci* **2012**, *7*, e13.
- [5] Zhang, Y.; Huang, B.; Yu, F.; Yuan, Q.; Gu, M.; Ji, J.; Zhang, Y.; Li, Y. 3D nitrogen-doped graphite foam@Prussian blue: an electrochemical sensing platform for highly sensitive determination of H₂O₂ and glucose. *Microchimica Acta* **2018**, *185*, 2–9.
- [6] Sheng, Q.; Zhang, D.; Shen, Y.; Zheng, J. Synthesis of hollow Prussian blue cubes as an electrocatalyst for the reduction of hydrogen peroxide. *Frontiers of Materials Science* **2017**, *11*, 147–154.
- [7] You, J. M.; Jeong, Y. N.; Ahmed, M. S.; Kim, S. K.; Choi, H. C.; Jeon, S. Reductive determination of hydrogen peroxide with MWCNTs-Pd nanoparticles on a modified glassy carbon electrode. *Biosensors and Bioelectronics* **2011**, *26*, 2287–2291.
- [8] Wang, H.; Wu, X.; Zhang, K.; Xu, J.; Zhang, L.; Zhuo, X.; Shi, H.; Qin, M.; Wang, C.; Zhang, N. Simple strategy for fabricating a Prussian blue/chitosan/carbon nanotube composite and its application for the sensitive determination of hydrogen peroxide. *Micro & Nano Letters* **2016**, *12*, 23–26.

- [9] Bard, A. J.; Faulkner, L. R.; Leddy, J.; Zoski, C. G. *Electrochemical methods: fundamentals and applications*; Wiley New York, 1980; Vol. 2; pp A25, 812–813.
- [10] Turner, A.; Karube, I.; Wilson, G. S. *Biosensors: fundamentals and applications*; Oxford university press, 1987; pp 3–11, 87–97.
- [11] Nasirizadeh, N.; Shekari, Z.; Nazari, A.; Tabatabaee, M. Fabrication of a novel electrochemical sensor for determination of hydrogen peroxide in different fruit juice samples. *Journal of food and drug analysis* **2016**, *24*, 72–82.
- [12] Chen, W.; Cai, S.; Ren, Q.-Q.; Wen, W.; Zhao, Y.-D. Recent advances in electrochemical sensing for hydrogen peroxide: a review. *Analyst* **2012**, *137*, 49–58.
- [13] Herren, F.; Fischer, P.; Ludi, A.; Hälg, W. Neutron diffraction study of Prussian Blue, $\text{Fe}_4[\text{Fe}(\text{CN})_6]_3 \cdot x\text{H}_2\text{O}$. Location of water molecules and long-range magnetic order. *Inorganic Chemistry* **1980**, *19*, 956–959.
- [14] Ge, C. X.; Li, P. J.; Lai, J. H.; Qiu, P. In situ synthesis and characterization of Prussian blue nanocubes on graphene oxide and its application for H_2O_2 reduction. *Indian Journal of Chemistry - Section A Inorganic, Physical, Theoretical and Analytical Chemistry* **2018**, *57A*, 26–33.
- [15] Christoph, S. Information about nanomaterials and their safety assessment: Zirconium dioxide - Material Information. <https://www.nanopartikel.info/en/nanoinfo/materials/zirconium-dioxide/material-informationliteratur> (accessed February 16, 2019).
- [16] Berry, F. J.; Skinner, S. J.; Bell, I. M.; Clark, R. J.; Ponton, C. B. The influence of pH on zirconia formed from zirconium (IV) acetate solution: Characterization by X-ray powder diffraction and Raman spectroscopy. *Journal of Solid State Chemistry* **1999**, *145*, 394–400.
- [17] Liu, W.-W.; Chai, S.-P.; Mohamed, A. R.; Hashim, U. Synthesis and characterization of graphene and carbon nanotubes: a review on the past and recent developments. *Journal of Industrial and Engineering Chemistry* **2014**, *20*, 1171–1185.
- [18] Ullah, I. Carbon nanotube membranes for water purification: Developments, challenges, and prospects for the future. *Separation and Purification Technology* **2018**, *209*, 307–337.
- [19] Iijima, S. Helical microtubules of graphitic carbon. *nature* **1991**, *354*, 56.

- [20] Schroeder, V.; Savagatrup, S.; He, M.; Lin, S.; Swager, T. M. Carbon nanotube chemical sensors. *Chemical reviews* **2018**, *119*, 599–663.
- [21] Tasis, D.; Tagmatarchis, N.; Bianco, A.; Prato, M. Chemistry of carbon nanotubes. *Chemical reviews* **2006**, *106*, 1105–1136.
- [22] Lawal, A. T. Synthesis and utilization of carbon nanotubes for fabrication of electrochemical biosensors. *Materials Research Bulletin* **2016**, *73*, 308–350.
- [23] Chen, R. J.; Zhang, Y.; Wang, D.; Dai, H. Noncovalent sidewall functionalization of single-walled carbon nanotubes for protein immobilization. *Journal of the American Chemical Society* **2001**, *123*, 3838–3839.
- [24] Bilalis, P.; Katsigiannopoulos, D.; Avgeropoulos, A.; Sakellariou, G. Non-covalent functionalization of carbon nanotubes with polymers. *RSC Advances* **2014**, *4*, 2911–2934.
- [25] Zhan, K.; Liu, H.; Zhang, H.; Chen, Y.; Ni, H.; Wu, M.; Sun, D.; Chen, Y. A facile method for the immobilization of myoglobin on multi-walled carbon nanotubes: poly (methacrylic acid-co-acrylamide) nanocomposite and its application for direct bio-detection of H₂O₂. *Journal of Electroanalytical Chemistry* **2014**, *724*, 80–86.
- [26] Guldi, D. M.; Martín, N. *Carbon nanotubes and related structures: synthesis, characterization, functionalization, and applications*; John Wiley & Sons, 2010.
- [27] Hirsch, A.; Vostrowsky, O. *Functional molecular nanostructures*; Springer, 2005; pp 193–237.
- [28] Wang, F.; Swager, T. M. Diverse chemiresistors based upon covalently modified multiwalled carbon nanotubes. *Journal of the American Chemical Society* **2011**, *133*, 11181–11193.
- [29] Huang, J.; Ng, A. L.; Piao, Y.; Chen, C.-F.; Green, A. A.; Sun, C.-F.; Hersam, M. C.; Lee, C. S.; Wang, Y. Covalently functionalized double-walled carbon nanotubes combine high sensitivity and selectivity in the electrical detection of small molecules. *Journal of the American Chemical Society* **2013**, *135*, 2306–2312.
- [30] Anastasescu, C.; Mihaiu, S.; Preda, S.; Zaharescu, M. *1D Oxide Nanostructures Obtained by Sol-Gel and Hydrothermal Methods*; Springer, 2016; pp 5–8.
- [31] Kayvani Fard, A.; Rhadfi, T.; McKay, G.; Al-marri, M.; Abdala, A.; Hilal, N.; Hussien, M. A. Enhancing oil removal from water using ferric oxide nanoparticles doped carbon nanotubes adsorbents. *Chemical Engineering Journal* **2016**, *293*, 90–101.

- [32] Ma, W.; Tian, D. Direct electron transfer and electrocatalysis of hemoglobin in ZnO coated multiwalled carbon nanotubes and Nafion composite matrix. *Bioelectrochemistry* **2010**, *78*, 106–112.
- [33] Brinker, C. J.; Scherer, G. W. *The physics and chemistry of sol-gel processing*; Academic press, 1989; Vol. 3; pp 115–119.
- [34] Zhao, H.; Xu, X.; Zhang, J.; Zheng, W.; Zheng, Y. Carbon nanotube–hydroxyapatite–hemoglobin nanocomposites with high bioelectrocatalytic activity. *Bioelectrochemistry* **2010**, *78*, 124–129.
- [35] Hobbs, J. M.; Patel, N. N.; Kim, D. W.; Rugutt, J. K.; Wanekaya, A. K. Glucose determination in beverages using carbon nanotube modified biosensor: an experiment for the undergraduate laboratory. *Journal of Chemical Education* **2013**, *90*, 1222–1226.
- [36] Wei, X.-P.; Luo, Y.-L.; Xu, F.; Chen, Y.-S.; Yang, L.-H. In-situ non-covalent dressing of multi-walled carbon nanotubes@ titanium dioxides with carboxymethyl chitosan nanocomposite electrochemical sensors for detection of pesticide residues. *Materials & Design* **2016**, *111*, 445–452.
- [37] Talari, A. C. S.; Martinez, M. A.; Movasaghi, Z.; Rehman, S.; Rehman, I. U. Advances in Fourier transform infrared (FTIR) spectroscopy of biological tissues. *Applied Spectroscopy Reviews* **2017**, *52*, 456–506.
- [38] Bunaciu, A. A.; gabriela Udristioiu, E.; Aboul-Enein, H. Y. X-Ray Diffraction: Instrumentation and Applications. *Critical Reviews in Analytical Chemistry* **2015**, *45*, 289–299.
- [39] Harris, D. C. *Quantitative chemical analysis*; Macmillan, 2010; pp 361–369.
- [40] Elgrishi, N.; Rountree, K. J.; McCarthy, B. D.; Rountree, E. S.; Eisenhart, T. T.; Dempsey, J. L. A Practical Beginner's Guide to Cyclic Voltammetry. *Journal of Chemical Education* **2017**, *95*, 197–206.
- [41] Savéant, J.-M. *Elements of molecular and biomolecular electrochemistry: an electrochemical approach to electron transfer chemistry*; John Wiley & Sons, 2006; Vol. 13.
- [42] Sarmiento, Y. Obtención y caracterización de sistemas nanoestructurados basados en nanotubos de carbono recubiertos con titania, zirconia e hidroxiapatita. *Universidad Central de Venezuela* **2011**,
- [43] Huber, L. *Validation and qualification in analytical laboratories*; CRC Press, 2007; pp 145–154.

- [44] Zhang, M.; Yuan, R.; Chai, Y.; Li, W.; Zhong, H.; Wang, C. Glucose biosensor based on titanium dioxide-multiwall carbon nanotubes-chitosan composite and functionalized gold nanoparticles. *Bioprocess and biosystems engineering* **2011**, *34*, 1143–1150.
- [45] Salam, M. A.; Burk, R. Synthesis and characterization of multi-walled carbon nanotubes modified with octadecylamine and polyethylene glycol. *Arabian Journal of Chemistry* **2017**, *10*, S921–S927.
- [46] Aqel, A.; El-Nour, K. M. A.; Ammar, R. A.; Al-Warthan, A. Carbon nanotubes, science and technology part (I) structure, synthesis and characterisation. *Arabian Journal of Chemistry* **2012**, *5*, 1–23.
- [47] Li, Z. Q.; Lu, C. J.; Xia, Z. P.; Zhou, Y.; Luo, Z. X-ray diffraction patterns of graphite and turbostratic carbon. *Carbon* **2007**, *45*, 1686–1695.
- [48] Luo, T. Y.; Liang, T. X.; Li, C. S. Addition of carbon nanotubes during the preparation of zirconia nanoparticles: Influence on structure and phase composition. *Powder Technology* **2004**, *139*, 118–122.
- [49] Dekanski, A.; Stevanović, J.; Stevanović, R.; Nikolić, B. Ž.; Jovanović, V. M. Glassy carbon electrodes. *Carbon* **2001**, *39*, 1195–1205.
- [50] Akinoglu, E. M.; Kätelhön, E.; Pampel, J.; Ban, Z.; Antonietti, M.; Compton, R. G.; Giersig, M. Nanoscopic carbon electrodes: Structure, electrical properties and application for electrochemistry. *Carbon* **2018**, *130*, 768–774.
- [51] Chakraborty, S.; Chattopadhyay, J.; Peng, H.; Chen, Z.; Mukherjee, A.; Arvidson, R. S.; Hauge, R. H.; Billups, W. E. Surface area measurement of functionalized single-walled carbon nanotubes. *Journal of Physical Chemistry B* **2006**, *110*, 24812–24815.
- [52] Fan, L.; Li, H.; Han, S.; Zhu, S.; Xu, G.; Liu, X.; Shi, L. Determination of concentrated hydrogen peroxide at single-walled carbon nanohorn paste electrode. *Electrochemistry Communications* **2008**, *10*, 695–698.
- [53] Hirsch, A.; Vostrowsky, O. *Functional molecular nanostructures*; Springer, 2005; pp 193–237.
- [54] Lousada, C. M.; Jonsson, M. Kinetics, mechanism, and activation energy of H₂O₂ decomposition on the surface of ZrO₂. *The Journal of Physical Chemistry C* **2010**, *114*, 11202–11208.
- [55] Lousada, C. M.; Johansson, A. J.; Brinck, T.; Jonsson, M. Mechanism of H₂O₂ decomposition on transition metal oxide surfaces. *The Journal of Physical Chemistry C* **2012**, *116*, 9533–9543.

- [56] Barreiro Fidalgo, A.; Dahlgren, B.; Brinck, T.; Jonsson, M. Surface reactions of H_2O_2 , H_2 , and O_2 in aqueous systems containing ZrO_2 . *Journal of Physical Chemistry C* **2016**, *120*, 1609–1614.

Abbreviations

$E^{\circ'}$ formal peak potential 18, 19

E_{pa} anodic peak potential 19

E_{pc} cathodic peak potential 19

ΔE_p peak-to-peak separation 18, 37

ν scan rate 26

$\nu^{1/2}$ root square of scan rate 18, 19

i_p peak current 18, 19

i_{pa} anodic peak current 18

i_{pa}/i_{pc} ratio of redox peak current 18

i_{pc} cathodic peak current 18

ZrO₂-CNT zirconia doped carbon nanotube 22, 61

AFM atomic force microscopy 10

CA chronoamperometry 19, 20

CNT carbon nanotube 2, 9–12, 14, 21, 23–25, 27, 31, 61

CV cyclic voltammetry 16–18, 37

DI distilled water 21

DMF *N,N*-Dimethylformamide 21, 22

DWCNT double-wall carbon nanotube 11, 12

FTIR fourier transform infraed 15, 25

GC glassy carbon 26–29, 61

HA hydroxyapatite 14

Hb hemoglobin 13, 14

LOD limit of detection 27

MWCNT multiwall carbon nanotube 9–11, 13, 14

NP nanoparticle 41

PB Prussian blue 2, 28, 29

PBS phosphate buffer saline 22, 26, 29

PDDA poly(diallyldimethylammonium chloride) 21, 22, 27, 29

SWCNT single-wall carbon nanotube 9

TEM transmission electron microscopy 10, 15, 25, 35

XRD x-ray diffraction 16, 25